

UNCLASSIFIED

AD 400 562

*Reproduced
by the*

ARMED SERVICES TECHNICAL INFORMATION AGENCY
ARLINGTON HALL STATION
ARLINGTON 12, VIRGINIA



UNCLASSIFIED

NOTICE: When government or other drawings, specifications or other data are used for any purpose other than in connection with a definitely related government procurement operation, the U. S. Government thereby incurs no responsibility, nor any obligation whatsoever; and the fact that the Government may have formulated, furnished, or in any way supplied the said drawings, specifications, or other data is not to be regarded by implication or otherwise as in any manner licensing the holder or any other person or corporation, or conveying any rights or permission to manufacture, use or sell any patented invention that may in any way be related thereto.

MIT Fluid Dynamics Research
Laboratory Report No. 63-1

EXPERIMENTS ON CYLINDER DRAG,
SPHERE DRAG, AND STABILITY IN
RECTILINEAR COUETTE FLOW

DAVID L. KOHLMAN

MASSACHUSETTS INSTITUTE OF TECHNOLOGY

MARCH 1963

SPONSORED BY THE
U. S. AIR FORCE OFFICE OF SCIENTIFIC RESEARCH
GRANT NO. AF-OSR-62-187 AND
GRANT NO. AF-OSR-156-63

400 562

710 562

MIT Fluid Dynamics Research
Laboratory Report No. 63-1

EXPERIMENTS ON CYLINDER DRAG,
SPHERE DRAG AND STABILITY IN
RECTILINEAR COUETTE FLOW

by

David L. Kohlman

Massachusetts Institute of Technology

March 1963

Sponsored by the
U. S. Air Force Office of Scientific Research
under AF-OSR-62-187



EXPERIMENTS ON CYLINDER DRAG, SPHERE DRAG,
AND STABILITY IN RECTILINEAR COUETTE FLOW

by

David L. Kohlman

ABSTRACT

The purpose of this study was to develop an apparatus for investigation of phenomena in rectilinear Couette flow, and to conduct experiments in several such areas. The project was divided into four main parts:

- (1) Design and development of the shear flow tank and related experimental apparatus.
- (2) Study of circular cylinder drag in Couette flow at low Reynolds number.
- (3) Study of sphere drag in Couette flow at low Reynolds number.
- (4) Study of instability of rectilinear Couette flow.

A historical and theoretical background for the present study is given.

The limited validity of Lamb's drag law for circular cylinders in a finite channel is demonstrated. As the Reynolds number decreases the walls cause a transition from Oseen flow to Stokes flow. Empirical drag formulas are presented.

Stokes formula for sphere drag in uniform flow is shown also to be valid in uniform shear flow. Measurements of sphere rotation rates in shear flow are presented.

Stability studies indicate that rectilinear Couette flow becomes unstable in the range $10^3 < Re_s < 10^4$. The primary disturbance is a series of vortices midway between the walls whose wavelength decreases with increasing Re_s . Though quantitative results are not entirely conclusive, the practical foundation is laid for further study and experimentation in this area. Recommendations and improvements are suggested which it is hoped will lead to more successful experimentation and understanding of this problem.

ACKNOWLEDGEMENTS

The author would like to express his sincere thanks to Professor Erik Mollo-Christensen for his valuable guidance and assistance as thesis advisor. The interest of Professor Leon Trilling and Professor James Daily, who served on the thesis committee, is also appreciated.

The cooperation and assistance of Mr. Charles Conn of Educational Services Incorporated is gratefully acknowledged. The photographs in Figure 13 are from the film "Kinematics of Deformation" being produced by Educational Services Incorporated and the National Committee for Fluid Mechanics Films.

Mr. George Falla rendered invaluable assistance in the photographic phases of the experiments. The manuscript was typed by Miss Katherine Palmer.

The work described in this report was sponsored by AFOSR under AF-GSR-62-187.

TABLE OF CONTENTS

<u>Chapter No.</u>		
I	<u>Introduction</u>	1
II	<u>Theory</u>	7
	2.1 Stokes Equations	7
	2.2 Oseen's Equations	10
	2.3 Flow Past a Sphere	12
III	<u>Experimental Apparatus</u>	25
	3.1 Shear Flow Tank	25
	3.1.1 Introduction	25
	3.1.2 Description of Apparatus	28
	3.1.3 Calibration and Performance	30
	3.1.4 Applications	35
	3.2 Balance System	37
	3.3 Measurement of Fluid Characteristics	38
IV	<u>Drag of a Circular Cylinder</u>	40
	4.1 Theoretical Considerations	40
	4.2 Experimental Investigation	46
	4.2.1 Introduction	46
	4.2.2 Finite Length Effects	48

	4.2.3 Results	49
V	<u>Drag of a Sphere</u>	55
	5.1 Introduction	55
	5.2 Experimental Apparatus	56
	5.3 Results	57
	5.4 Analysis of Interference Effects	58
	5.5 Free Rotation of a Sphere in Shear Flow	60
VI	<u>Investigation of Shear Flow Characteristics</u>	
	6.1 Introduction	62
	6.2 Experiments	62
	6.2.1 Effect of Test Section Length-Width Ratio	62
	6.2.2 Instability of Couette Flow	64
	6.3 Discussion	67
VII	<u>Discussion and Conclusions</u>	76
	7.1 Experimental Apparatus	76
	7.2 Cylinder Drag, Sphere Drag, and Stability	77
	<u>Appendices</u>	
A	<u>Details of Calculation of Experimental Drag</u>	81
	A.1 Circular Cylinder Drag	81
	A.2 Sphere Drag	82

B	<u>Accuracy of Experimental Data</u>	83
	B.1 Accuracy of Individual Measurements	83
	B.2 Accuracy of Final Results	85

References

LIST OF FIGURES

<u>Figure No.</u>		<u>Page</u>
1	Drag Coefficient of a Sphere in Uniform Flow	97
2	Schematic Drawing of Reichardt's Shear Flow Tank	98
3	General Arrangement of Shear Flow Tank Components	99
4	Details of Belt, Roller, and Supporting Plate Arrangement	100
5	Photograph of Tank 1	101
6	Photograph of Tank 2	102
7	Velocity Profile in Test Section at Surface $Re_s = 28$	103
8	Velocity Profile in Test Section at Surface $Re_s = 48$	104
9	Velocity Profile in Test Section, $Re_s = 55$	105
10	Velocity Profile With One Belt Stationary, $\frac{A}{H} = 4.65$	106
11	Streak Photographs of Shear Flow With One Belt Stationary, $\frac{A}{H} = 13$	107
12	Velocity Profiles With One Belt Stationary, $\frac{A}{H} = 13$	108
13	Deformation of a Surface Pattern in Rectilinear Couette Flow	109
14	Velocity Profiles in Planes Parallel to the Belts, Tank 2	112
15	Approximate Depth of Two-Dimensional Flow, Tank 2	113
16	Typical Vertical Velocity Profile Photograph	114
17	Symmetric Shear Flow Past a Circular Cylinder	115

18	Symmetric Shear Flow Past a Circular Cylinder	116
19	Schematic Drawing of Beam Balance	117
20	Photograph of Balance System	118
21	Test Setup, Tank 2	119
22	Cannon-Fenske Viscometers	120
23	Drag Coefficient of a Circular Cylinder in Uniform Flow	121
24	Cylinders Used in Drag Experiments	122
25	Effect of Aspect Ratio on Drag of a Circular Cylinder, $d = .0074$, $\frac{y}{H} = \frac{1}{3}$	123
26	Effect of Aspect Ratio on Drag of a Circular Cylinder, $d = .039$, $\frac{y}{H} = \frac{1}{3}$	124
27	Drag of a Circular Cylinder Between Parallel Walls in Shearing Flow, $\frac{y}{H} = \frac{1}{3}$	125
28	Drag of a Circular Cylinder Between Parallel Walls in Shearing Flow, $\frac{y}{H} = \frac{1}{3}$	126
29	Drag of a Circular Cylinder Between Parallel Walls in Stokes Flow, $\frac{y}{H} = \frac{1}{3}$	127
30	Effect of Lateral Position on Drag of a Circular Cylinder Between Parallel Walls in Stokes Flow	128
31	Geometry of Sphere and Cylinder Mounting	129
32	Spheres Used in Drag Tests	130
33	Drag of a Sphere in Shear Flow	131
34	Drag of a Sphere in Shear Flow	132
35	Drag of a Sphere in Shear Flow	133

36	Rotation Rate of a Free Sphere in Uniform Shear Flow	134
37	Streak Photographs of Shear Flow, $\frac{\Delta}{H} = 13$	135
38	Streak Photograph of Shear Flow, $\frac{\Delta}{H} = 13$	136
39	Velocity Profiles, $\frac{\Delta}{H} = 13$	137
40	Velocity Profile, $\frac{\Delta}{H} = 13$	138
41	Streak Photographs of Rectilinear Couette Flow	139
42	Streak Photographs of Rectilinear Couette Flow	140
43	Streak Photographs of Rectilinear Couette Flow	141
44	Wavelength and Wave Number of Primary Instability in Couette Flow	142
45	Modes of Oscillations in Plane Couette Flow (Hopf)	143
46	Stability Characteristics in Parallel Stream Mixing Region (Lessen)	144

SYMBOLS

p	pressure
ρ	density
μ	viscosity
ν	kinematic viscosity,
x, y, z	Cartesian coordinates
u, v, w	velocity components in Cartesian coordinates
r, θ, ϕ	polar coordinates
v_r, v_θ, v_ϕ	polar velocity components
ψ	Stokes stream function
U	rectilinear velocity in test section
U_0	belt velocity
V	undisturbed relative velocity at center of cylinder or sphere
S	rate of shear
a	sphere radius
d_s	sphere diameter
d_c	cylinder diameter
L	cylinder length
Λ	test section length
H	test section width

h	distance of sphere from a boundary
ω	angular velocity
M	angular moment
D	drag
Re	Reynolds number based on velocity, V
Re _S	Reynolds number based on shear, S and sphere or cylinder diameter, d
Re _T	Reynolds number at which Lamb's law becomes invalid
α	drag coefficient based on viscous forces, $D/\mu VL$
C _D	drag coefficient based on inertia forces, $D/\frac{1}{2} \rho V^2(\text{area})$
log	logarithm to the base 10
ln	logarithm to the base e
K	empirically determined constant in cylinder drag law
c	constant in Brenner's boundary correction formula
λ	wavelength of a disturbance
δ	wave number, $\frac{2\pi}{\lambda}$
δ	boundary layer thickness
Re _s	Reynolds number based on shear, S and test section width, H

CHAPTER I

INTRODUCTION

One of the oldest branches of fluid mechanics is that of very low Reynolds number flow. G. G. Stokes (1) first formulated the equations governing pure viscous flow (in which all inertia forces are negligibly small) in 1851. This flow regime, now known as Stokes flow, in practically all cases is limited to Reynolds numbers less than unity.

Since Stokes' first paper, this subject has received the attention of many investigators. However, there is still a considerable amount of interest in low Reynolds number flow, because of the many interesting unsolved problems which have direct applications to modern fluid dynamics. A great many meteorological, sedimentation, and chemical colloid phenomena occur in this regime, and Hoglund (2) points out that "Reynolds numbers of interest in gas-particle rocket nozzle flows are usually in the range 0 to 100."

After Stokes formulated his equations, the only fluid flow regimes which yielded readily to analysis were the two limiting cases of potential flow, which neglects viscous forces ($Re = \infty$), and Stokes flow, which neglects inertia forces ($Re = 0$). Except for a few very special cases, the vast area inbetween, governed by the complete, non-linear Navier-Stokes equations was largely mathematically intractable.

A major improvement to this situation was made by Prandtl (3) in 1904 with his well-known boundary layer theory. This theory made it possible to analyze flows with Reynolds numbers as low as 10^4 and higher, thus opening great areas for analysis in the upper end of the scale.

Progress at the lower end of the Reynolds number scale has proceeded in a far less spectacular and successful manner. The first improvement to Stokes equations was made by Oseen (4) in 1910, in which he took into account linearized terms for the inertia forces at large distances from a body. Even though this technique provides a uniformly valid approximation to the velocity and all its derivatives (Stokes equations give a uniformly valid approximation to the velocity only) and provides a satisfactory solution to the

two-dimensional flow past an infinite circular cylinder (Stokes equations yield no solution in this case), the Reynolds number of validity is scarcely extended above unity.

Since the work of Oseen (5), most attempts to obtain analytical solutions for flows at higher Reynolds numbers than are valid for his equations have consisted of separate infinite expansions for flow regions near to and far away from the body, which are matched in a common region of overlap. Several investigators have used variations of this approach (6, 7, 8, 9). This has provided reliable analytical data (such as drag coefficients) up to $Re \leq 4$. The only other technique successfully employed has been a numerical solution of the Navier-Stokes equations by electronic computer, using relaxation techniques. While perhaps lacking generality and being somewhat limited in scope, this method has provided valuable insight into phenomena significant to this Reynolds number range, such as separation, vortex formation, and vorticity distribution (10, 11, 12). In many respects, numerical solutions by relaxation and finite difference techniques appear to be the most promising theoretical approach to the intermediate Reynolds number range.

In spite of the progress that has been made, most of the theoretical approaches have been very limited due to their complexity and the lengthy, laborious calculations required. Because of this, and the large Reynolds number gap between the Oseen regime and the boundary layer regime, experimental methods have been relied upon quite extensively. Even so, experimental progress has been surprisingly slow, and there are many areas where practically no data exists. For instance, Lamb's equation (13) for the drag of a circular cylinder in a uniform stream, based on Oseen's equations was not verified until 1953, and then only to $Re \geq .06$, (14).

In many cases, the existing data is misinterpreted and its limitations overlooked. An example of this is found in Ref. 50 which demonstrates the large effect density ratio between body and fluid has on the apparent drag coefficient of a body in free fall. Hence, there is still a need for considerable experimental data in the low Reynolds number regime.

One area that has received practically no analysis is that of shearing flows, even though in practice this case occurs far more often than uniform flow.

Hoglund (2) points out that particle rotation and shearing flow can significantly influence particle motion in a rocket nozzle. The entrainment and circulation of ground debris by ground effect machines and helicopters is strongly dependent on the forces on particles in the ground shear layer. This problem has been investigated by Vidal (15) but he has entirely neglected viscous effects which can be significant under certain conditions. Several other investigators have treated shear flows past bodies (16, 17, 18) but unfortunately these are restricted to inviscid flow.

Theoretical analysis of shear flow past bodies at low Reynolds numbers has been limited by the mathematical difficulties encountered. Experimental investigations have been hampered by the lack of a method of generating rectilinear simple shear flows in the laboratory on a reasonably large scale. At present, there is virtually no experimental data on force coefficients of bodies in viscous shear flow.

The purpose of this thesis is twofold. The first objective was to design and develop the equipment and techniques necessary for experimental investigation of rectilinear shear flows and of various bodies immersed in shear flow. The second was to conduct an experimental

investigation of several cases to check theoretical solutions where they exist, and to present original experimental data where there is no information available to date.

A thorough analysis of the theoretical history and background for the investigation of low Reynolds number flow is given in Chapter II, along with suggestions of additional parameters which arise in the case of shearing flows.

Chapter III describes in detail the design and construction of the experimental apparatus used. Of particular interest is the unique flow tank in which a two-dimensional linear shear flow is generated by means of a system of moving belts.

Further chapters describe experimental investigations of the drag of circular cylinders in shear flows, the drag of spheres in shear flows, and rotation rates of free spheres as a function of shear rate and Reynolds number. An investigation was made of the characteristics of instability of the shear flow leading eventually to turbulence.

Test results are presented for Reynolds numbers varying from 6.6×10^{-4} to 1.8 based on cylinder or sphere diameter. All forces have been measured directly by means of a simple beam balance system.

CHAPTER II

THEORY2.1 Stokes Equations

In 1851, Stokes (1) formulated his famous equations for very viscous flow. They represent the asymptotic approximation to the Navier-Stokes equations as $Re \rightarrow 0$. One obtains Stokes equations by neglecting the inertia terms (which are negligibly small compared to viscous terms) in the incompressible, steady flow, Navier-Stokes equations. This gives the following system of equations:

$$\begin{aligned} \frac{\partial p}{\partial x} &= \mu \left(\frac{\partial^2 u}{\partial x^2} + \frac{\partial^2 u}{\partial y^2} + \frac{\partial^2 u}{\partial z^2} \right) \\ \frac{\partial p}{\partial y} &= \mu \left(\frac{\partial^2 v}{\partial x^2} + \frac{\partial^2 v}{\partial y^2} + \frac{\partial^2 v}{\partial z^2} \right) \\ \frac{\partial p}{\partial z} &= \mu \left(\frac{\partial^2 w}{\partial x^2} + \frac{\partial^2 w}{\partial y^2} + \frac{\partial^2 w}{\partial z^2} \right) \end{aligned} \quad (2.1)$$

along with the equation of continuity,

$$\frac{\partial u}{\partial x} + \frac{\partial v}{\partial y} + \frac{\partial w}{\partial z} = 0 \quad (2.2)$$

Hereafter, flow which is governed by Stokes equations, 2.1 and 2.2, will be called "Stokes flow." It is important to note that Stokes equations are linear in both velocity and pressure, thus solutions to Stokes equations may be superposed in both velocity and pressure. Another interesting characteristic is that for Stokes flow past a symmetrical body (fore and aft) the streamlines in front of and behind the body must be symmetrical, for by reversing the direction of flow, i.e., by changing the sign of the velocity components and pressure gradients in equations 2.1 and 2.2, the system is transformed into itself.

As with all asymptotically approximate systems, the important question of validity must be considered. Stokes equations give exact solutions only for $Re = 0$. In reality, of course, the Reynolds number must always have some finite, though small, value.

Any body moving through a viscous fluid must experience some resistance. Hence, if we consider the momentum flux across a large surface surrounding the body, it is clear that the magnitude of the perturbation velocity cannot fall to zero more rapidly than the inverse square of the distance from the body. But the acceleration of the fluid (proportional to inertia force) is a

constant multiple of the first derivative of the velocity, while the viscous forces are a multiple of the second derivative of the velocity. Thus the viscous forces can dominate everywhere only if the perturbation velocities decay exponentially. Since they clearly do not, we are faced with the inconsistency that a solution to Stokes equations (at large distances from the body) violates the very assumptions on which the equations are formulated. In mathematical terms, Stokes solution does not provide a uniformly valid approximation to all the required properties of the flow for a small non-zero Reynolds number perturbation because of a singularity at infinity.

Fortunately, however, it can be shown that the solution does provide a uniformly valid approximation to the total velocity distribution, but not the derivatives, which are in error at large distances from the body (6). Thus, one may safely evaluate bulk properties of the flow, such as drag (see section 2.3).

The foregoing limitations were realized by Oseen (5) in 1910. Accordingly, he proposed the following improvement.

2.2 Oseen's Equations

Since the inertia forces are important only at large distances from the body, Oseen included a linearized inertia term which accounts for them at large distances, but remains small close to the body where the viscous terms clearly continue to dominate. For the remote boundary condition of a uniform stream with a velocity, U_∞ , Oseen's equations are

$$\left. \begin{aligned}
 \rho U_\infty \frac{\partial u}{\partial x} + \frac{\partial p}{\partial x} &= \mu \nabla^2 u \\
 \rho U_\infty \frac{\partial v}{\partial x} + \frac{\partial p}{\partial y} &= \mu \nabla^2 v \\
 \rho U_\infty \frac{\partial w}{\partial x} + \frac{\partial p}{\partial z} &= \mu \nabla^2 w
 \end{aligned} \right\} \quad (2.3)$$

$$\frac{\partial u}{\partial x} + \frac{\partial v}{\partial y} + \frac{\partial w}{\partial z} = 0$$

Flow governed by these equations will be called "Oseen flow."

Clearly, equations (2.3) are still linear in pressure and velocity, but there is now another parameter involved, the freestream velocity, U_∞ . Thus solutions of the Oseen equations may not be superposed unless they are both with respect to the same freestream uniform velocity.

By changing the signs of the velocities and pressure gradients in (2.3) we observe that the equations do not transform into themselves, so Oseen flow about a symmetrical body does not have symmetrical streamlines. Instead, the familiar wake characteristics appear.

Proudman and Pearson (6) point out a popular misconception concerning Oseen's equations. Consider the velocity components to be written as $u = U_{\infty} + u'$, $v = v'$, $w = w'$, where u' , v' , and w' are perturbations to the uniform flow. Now if the full incompressible Navier-Stokes equations are linearized with respect to the perturbation velocities, one obtains equations (2.3) identically. However, this interpretation is entirely wrong, and has resulted in misleading statements by such writers as Lamb (13) and Schlichting (19) to the effect that the equations are inaccurate near the body, where the boundary condition $u' = -U_{\infty}$ would make such a linearization ridiculous. Oseen's equations were not intended to give a uniform approximation to the inertia terms, and the difference between Oseen's and Stokes' theory near the body is of a small order, which neither theory is entitled to discuss.

In order to more clearly illustrate the characteristics, applications, and validity of the Stokes and Oseen equations, as well as further improvements, let us consider the specific problem of the flow past a sphere.

2.3 Flow Past a Sphere

The oldest known solution of Stokes equations was given by Stokes himself in his original paper (1), for the case of uniform parallel flow past a sphere. Details of the method of solution are given in both Lamb (13) and Landau and Lifshitz (20). For a sphere of radius a in a uniform stream of velocity U_∞ along the x-axis, the pressure and velocity components are given as

$$\begin{aligned} u &= U_\infty \left[\frac{3ax^2}{4r^3} \left(\frac{a^2}{r^2} - 1 \right) - \frac{a}{4r} \left(3 + \frac{a^2}{r^2} \right) + 1 \right] \\ v &= U_\infty \left[\frac{3axy}{4r^3} \left(\frac{a^2}{r^2} - 1 \right) \right] \\ w &= U_\infty \left[\frac{3axz}{4r^3} \left(\frac{a^2}{r^2} - 1 \right) \right] \\ p - p_\infty &= - \frac{3\mu U_\infty ax}{2r^3} \end{aligned} \quad (2.4)$$

Or, in spherical components,

$$\begin{aligned} V_r &= U_\infty \cos \theta \left[1 - \frac{3a}{2r} + \frac{a^3}{2r^3} \right] \\ V_\theta &= -U_\infty \sin \theta \left[1 - \frac{3a}{4r} - \frac{a^3}{4r^3} \right] \end{aligned} \quad (2.5)$$

Knowing the velocity and pressure fields it is a straightforward matter to compute the drag, which Stokes found to be

$$D = 6\pi\mu U_{\infty} a \quad (2.6)$$

One-third of the drag is due to the pressure field, the remaining two-thirds being a result of viscous stresses on the surface of the sphere.

In Stokes flow, it is common to use viscous force coefficients, in which forces are non-dimensionalized with respect to viscous terms rather than dynamic pressure as in the more familiar aerodynamic force coefficients. Stokes drag equation in non-dimensional form becomes

$$\alpha = \frac{D}{\mu U_{\infty} a} = 6\pi \quad (2.7)$$

Thus we can make the following generalizations which characterize the Stokes regime of flow:

1. The viscous drag coefficient, α , for a body is a constant.
2. The drag of a body is independent of fluid density.
3. The drag of a body is proportional to the first power of the viscosity and the relative velocity.

If we wish to use the more familiar drag coefficients based on dynamic pressure, we have

$$D = C_D \pi a^2 \frac{1}{2} \rho U_\infty^2 = 6\pi\mu U_\infty a$$

$$C_D = \frac{24}{Re} \quad ; \quad Re = \frac{2U_\infty a}{\nu} \quad (2.8)$$

Fig. 1 shows a comparison of Stokes drag curve, equation (2.8), compared with the results of several experimental investigations (38). Stokes drag is valid up to approximately $Re = .60$.

Now we can make a qualitative statement about the validity of Stokes equations since we have a specific solution. The inertia forces are proportional to $\rho u \partial u / \partial x$. From equations (2.5) we see that for large r , they are of order $\rho U_\infty^2 a / r^2$. Similarly the viscous forces being proportional to $\mu \partial^2 u / \partial y^2$, at large r are of order $\mu U_\infty a / r^3$. The Stokes theory becomes invalid when inertia and viscous forces become comparable, i.e.,

$$\frac{\rho U_\infty r}{\mu} = Re \frac{r}{2a} = O(1) \quad (2.9)$$

For very small Reynolds numbers, Stokes solution does not break down until r is very large and freestream conditions have almost been attained. Hence, as Proudman

and Pearson point out (6), although the higher derivatives are inaccurate at large distances, the total velocity field can be uniformly approximated.

Oseen provided the first improvement to Stokes drag law with a solution to his linearized equations (2.3) which account for the dominant inertia terms at large distances from the sphere. It is most easily expressed in the form of a Stokes stream function:

$$\psi = \frac{U_\infty}{4} \left[\left(2r^2 + \frac{a^3}{r} \right) \sin^2 \theta + \right. \\ \left. - \frac{3a^2}{2Re} (1 + \cos \theta) \left(1 - e^{-\frac{1}{2} Re \frac{r}{a} (1 - \cos \theta)} \right) \right] \quad (2.10)$$

Stokes solution, equations (2.5), may also be expressed in the same form, becoming

$$\psi = \frac{U_\infty}{4} \left(2r^2 - 3ar + \frac{a^3}{r} \right) \sin^2 \theta \quad (2.11)$$

Equation (2.10) satisfies Oseen's equations (2.3) and the boundary condition at infinity. When r is of order a (2.10) can be expressed in the form

$$\psi = \frac{U_\infty}{4} \left(2r^2 - 3ar + \frac{a^3}{r} \right) \sin^2 \theta + O(Re) \quad (2.12)$$

which agrees with Stokes solution and the relevant boundary condition on the sphere, to an adequate approximation.

To derive a solution of equations (2.3) which satisfies the boundary condition at the sphere exactly is very difficult, and of limited value in that the governing equations themselves involve approximations of the same order as those in the boundary conditions of the solution (2.10). And the solution of an equation, even though satisfying all boundary conditions exactly, can never be regarded as accurate to a higher order than that of the approximations made to formulate the original governing equations.

Using Oseen's solution for the velocity distribution, the drag on a sphere becomes

$$D = 6\pi\mu U_{\infty} a \left(1 + \frac{3U_{\infty} a}{8\nu} \right) \quad (2.13)$$

In terms of a drag coefficient, we have

$$C_D = \frac{24}{Re} \left(1 + \frac{3}{16} Re \right) \quad (2.14)$$

or

$$\alpha = 6\pi \left(1 + \frac{3}{16} Re \right)$$

which clearly reduces to Stokes law (2.8) as $Re \rightarrow 0$.

A graphical comparison of the Stokes and Oseen drag laws with experimental data is shown in Fig. 1. In spite of the increased accuracy with which the flow field is represented, Oseen's law is accurate only to approximately $Re = 1$, only a slight improvement to Stokes formula.

The next improvement in theoretical analysis for increasing Reynolds number was based on an expansion technique begun by Lagerstrom and Cole (6), and Lagerstrom and Kaplun (8) and developed further by Proudman and Pearson (7). This method develops locally valid expansions based on Oseen flow far from the body and Stokes flow close to the body. The two expansions are computed to satisfy their respective infinity and surface boundary conditions and are matched in a common region of overlap. This technique offers improved accuracy to Oseen solutions, but it also becomes invalid at relatively low Reynolds numbers since the two expansions eventually fail to have a common region of validity.

Using this method, Proudman and Pearson arrived at the following formula for the drag of a sphere in viscous uniform flow:

$$C_D = \frac{24}{Re} \left(1 + \frac{3}{16} Re + \frac{9}{160} Re^2 \ln\left(\frac{Re}{2}\right) + O\left(\frac{Re^2}{4}\right) \right) \quad (2.15)$$

Equation (2.15) which obviously reduces to both Oseen's and Stokes' drag formulas as $Re \rightarrow 0$, is accurate to approximately $Re = 1.6$ as shown in Fig. 1. Unfortunately, this offers very little improvement over Oseen's solution.

Further attempts to find more accurate analytical solutions have been based primarily on relaxation methods for numerically solving the governing equations.

Pearcy and McHugh (11) performed a numerical solution of Oseen's equations for the uniform flow past a sphere at $Re = 1, 4, \text{ and } 10$. Unfortunately such solutions provide little new information, since, as was pointed out earlier, Oseen's equations become increasingly inaccurate for $Re > 1$.

Jenson (12) carried out a numerical solution by relaxation techniques of the complete Navier-Stokes equations for uniform flow past a sphere. He presents solutions for $Re = 5, 10, 20, \text{ and } 40$. This method appears to be very effective in determining most of the characteristics of the flow field. Drag coefficients so determined match very well with experimental values. His results indicate that separation at the rear of the sphere begins at $Re = 17$.

Now consider the motion of a sphere in a shearing flow. If the Reynolds number is low enough that Stokes equations are valid, this case may be reduced to two simple flows which can be superimposed. Since both velocity and pressure are linear in Stokes' equations, one may add the forces directly as well as

the velocity fields. Hence constant shear flow (linear velocity profile) with a mean velocity V past a sphere can be considered to be the result of a uniform flow velocity, V , past the sphere superposed with a symmetric shear flow of zero mean velocity at the sphere. Since the symmetric shear flow produces only a moment, but no drag, the drag of a sphere in a constant shear flow with mean velocity, V , is merely

$$D = 6\pi\mu Va \quad (2.6)$$

as predicted by Stokes for uniform flow. It is also clear that if the sphere is rotating, one may again merely superpose the symmetric flow field for a sphere rotating in a fluid at rest. Since no drag is produced by pure rotation, equation (2.6) may still be used to predict the drag.

All of the above Stokes flow problems have been solved analytically. The uniform flow, solved by Stokes has already been given. Vand (21) and Jeffery (22) give a solution for symmetrical linear shear flow around a sphere which is rotating freely. To get the flow for a stationary sphere in shear flow, one merely subtracts the solution for a sphere rotating at zero mean velocity, given by Landau and Lifshitz (20).

For a sphere of radius a rotating about an axis perpendicular to the x - y plane at an angular velocity, ω , the velocity field is given by

$$u = -\frac{a^3}{r^3} \omega y$$

$$v = \frac{a^3}{r^3} \omega x$$
(2.16)

and the net moment on the sphere can easily be shown to be

$$M = -8a^3 \pi \mu \omega$$
(2.17)

Vand's solution for a freely rotating sphere in a linear shear with infinite boundary conditions

$$u = Sy, \quad v = 0, \quad w = 0$$
(2.18)

is given as

$$u = -\frac{S}{2} S \left[\frac{a^3 x^2 y}{r^5} \left(1 - \frac{a^2}{r^2}\right) \right] + Sy \left(1 - \frac{a^5}{2r^3}\right)$$

$$v = -\frac{S}{2} S \left[\frac{a^3 x y^2}{r^5} \left(1 - \frac{a^2}{r^2}\right) \right] - \frac{S a^5 x}{2 r^3}$$

$$w = -\frac{S}{2} S \left[\frac{a^3 x y z}{r^5} \left(1 - \frac{a^2}{r^2}\right) \right]$$
(2.19)

By setting $r = a$ in the above equations it is clear that the sphere is rotating with an angular velocity ω such that

$$\omega = -\frac{1}{2} S \quad (2.20)$$

Thus, to obtain the flow field for a stationary sphere in shear flow with a shear $S \text{ sec}^{-1}$, merely subtract equations (2.16) from equations (2.19) with $\omega = -S/2$.

For uniform flow it is usually sufficient to describe most phenomena in terms of the Reynolds number given as

$$Re = \frac{Vd}{\nu} \quad (2.21)$$

where V is the relative velocity and d a characteristic length. However, when the flow is shearing, another parameter, the shear S , must be included. For this case the mean velocity can even be zero. Thus it is proposed that a second Reynolds number based on shear be formulated as follows,

$$Re_s = \frac{Sd^2}{\nu} \quad (2.22)$$

A similar parameter was introduced by Taylor (40) in 1923, but it was defined in terms applicable only to the flow between rotating concentric cylinders.

It is obvious that for a constant Re based on mean velocity, such properties as drag, moment, etc., may vary widely as Re_S changes over a wide range. For pure Stokes flow, the influence of Re_S is negligible, but it becomes increasingly important as both Reynolds numbers are increased. Another parameter which may be of importance in shear flow is the ratio of body rotation to shear rate, ω/s .

One should also observe that for pure Stokes flow, there can be no transverse force developed on a sphere due to stream shear and/or sphere rotation because of the complete symmetry of all the component flow patterns. This may also be seen as the result of the fact that transverse forces in this case must be the result of inertia forces. But Stokes flow neglects completely all inertia terms.

Note, however, that as shown earlier, the inertia terms do exceed viscous terms at large distances from the body. But they do not affect the bulk properties, such as drag. However, it is quite possible that second or third order inertia terms may produce second or third order effects such as transverse forces which depend on the effects of inertia terms. An interesting

study by Rubinow and Keller (23) illustrates this phenomenon quite clearly. They used the expansion method of Proudman and Pearson to show that the lift on a sphere spinning at an angular velocity ω and moving with a velocity V through a viscous liquid is given by:

$$\text{Lift} = \pi \rho a^3 (\bar{\omega} \times \bar{V}) [1 + O(Re)] \quad (2.23)$$

This is clearly related to the familiar "Magnus effect", and is independent of viscosity to the first order. It is more instructive to form a lift-drag ratio to illustrate the relative magnitude of the forces.

As $Re \rightarrow 0$

$$\frac{\text{Lift}}{\text{Drag}} = \frac{\pi \rho a^3 \omega V}{6\pi \mu V a} = \frac{\rho a^2 \omega}{6\mu} = \frac{Re_\omega}{6} \quad (2.24)$$

$$\text{where } Re_\omega = \frac{\omega a^2}{\nu}$$

Thus for a given sphere and fluid, the lift/drag ratio is directly proportional to angular velocity ω . However, for decreasing Reynolds number based on ω , the lift/drag also decreases proportionately. This result applies only for uniform flow past a spinning sphere.

One must be very careful in applying the above results to actual situations for this reason. The lift is entirely the result of considering the inertia effects a large distance from the body. Thus the presence of a finite wall or boundary even far from the body which can alter or mask off the inertia terms will change the lift quite radically, while having virtually no effect on the primarily viscous effects such as drag. Unfortunately, such effects are most difficult to predict, but are quite significant, as is shown clearly in Chapter IV by the effect of a wall on an infinite circular cylinder. Because the region of significance of inertia terms moves farther and farther away from the body as Re decreases, and because the extent of a fluid is always finite, there is always some lower limit for the Reynolds number for which an analysis based on the effect of inertia terms must become invalid.

CHAPTER III

EXPERIMENTAL APPARATUS3.1 Shear Flow Tank

3.1.1 Introduction - The experimental program of this thesis required a rectilinear constant shear flow (linear velocity profile) which was large enough to generate measurable forces on test models suspended in the flow. Practically all previous attempts to analyze shear flow phenomena in the laboratory have made use of rotating concentric cylinders. Several investigators have used this technique, and a typical example of such a device is described in detail by Trevelyan and Mason (24).

When the gap between the cylinders is small compared to their diameters, a nearly linear shear flow exists between the cylinders which rotate at unequal angular velocities. The flow profile is not exactly linear because of centrifugal forces, and is easily found to be:

$$u(r) = \frac{1}{r_2^2 - r_1^2} \left[r(\omega_2 r_2^2 - \omega_1 r_1^2) - \frac{r_1^2 r_2^2}{r} (\omega_2 - \omega_1) \right] \quad (3.1)$$

Where u is the radial velocity, r is the radial distance from the axis of rotation, r_1 and r_2 are the radii, and ω_1 and ω_2 are the angular velocities of the inner and outer cylinders respectively. The radial distribution of shear then becomes

$$S = r \frac{d\left(\frac{u(r)}{r}\right)}{dr} = 2 \frac{(\omega_2 - \omega_1) r_1^2 r_2^2}{(r_2^2 - r_1^2) r^2} \quad (3.2)$$

But S must be constant throughout in a pure constant shear flow (Couette flow).

Besides this drawback, the gap between cylinders in most practical devices must be so small that wall effects predominate for anything larger than microscopic particles. This makes it almost impossible to generate measurable forces. Further difficulties result from the Taylor instability of flow between rotating cylinders, rendering this device virtually useless for studies of rectilinear shear flow stability, as well as interface stability in a shear flow.

Another method of producing a uniform shear flow was developed by Owen and Zienkiewicz (25). They installed a grid of rods in a wind tunnel upstream of the test section. By properly spacing the rods a linear shear flow superimposed on a mean flow was obtained. This same technique was used by Vidal (26) to obtain a nonuniform shear pattern in a wind tunnel. Though very successful for many applications, this method cannot be employed for low Reynolds number experiments. A further limitation results from the fact that a flow generated in this manner is turbulent, rather than laminar. Also, the flow must always be superimposed on a relatively high mean velocity.

The first successful technique of generating a low Reynolds number rectilinear shear flow was developed by Reichardt (27). He used a single endless belt rotating on two revolving drums as shown in Fig. 2. He found that a linear shear flow existed on the free surface between the two inner sides of the belt. His apparatus was used primarily for streak photo studies of flow patterns past cylinders and the effect of turbulence on the velocity profile (28). Although it has proved quite useful, it is felt that the Reichardt

apparatus has several disadvantages: (1) The end effects extend well into the test section. (2) It is very difficult to keep the belt perfectly plane and free of vibration as it moves past the test section. (3) Visual and physical access is limited to the free surface at the top of the tank. (4) Only a perfectly symmetrical flow with zero mean velocity can be generated. (5) Studies of interface stability in a shear flow are impossible.

The apparatus developed by the author and described in the following sections overcomes all of the difficulties mentioned above, and provides a very versatile technique for investigating phenomena associated with a shear flow.

3.1.2 Description of Apparatus - A schematic drawing of the apparatus is shown in Fig. 3. Four rollers are driven by a system of belts and pulleys from a variable speed drive. Each pair of rollers is supported by arms extending from flat plates. The plates provide rigid walls on each side of the test section and prevent vibrations and waves from developing in the flow generating belts. The belts, which are stretched over each pair of rollers, are made of rubber sheet.

The system is immersed in the fluid and induces the flow indicated by arrows in Fig. 3. It was necessary to perforate the rollers to prevent the fluid entrained between the moving belt and roller from acting as a lubricant and allowing slippage. This allows fluid to flow through the roller, rather than between the roller and the belt. In addition, it was found necessary to glue strips of abrasive cloth on the rollers to prevent slippage. This arrangement is shown in Fig. 4.

The plate supporting the driving belts on each side of the test section needed lubrication to allow the belts to slide smoothly. Therefore, a number of holes were drilled in the plates.

In the course of the investigation, two shear flow tanks were designed and built. The first one (Tank 1) was built to test the basic concept, and to refine the operational difficulties encountered. It was subsequently used for many of the experimental investigations of this thesis. The second, (Tank 2) was designed by the author at the request of Educational Services, Inc., for use in an educational movie on volume kinematics. It incorporated several improvements over Tank 1, primarily in mechanical details. There were also minor changes in dimensions. The tank itself was

constructed entirely of plexiglas, affording visual access to the test section from both ends, the bottom, and the top free surface. Table 3.1 gives a tabulation of the properties of both tanks. Figs. 5 and 6 are photographs of Tanks 1 and 2 respectively. Note that the entire system of belts and mechanisms are mounted on the removable lid of the tank, for convenient access.

3.1.3 Calibration and Performance - The apparatus used aqueous glycerol as a working fluid. By changing the relative concentration of water and glycerine, the viscosity could be varied by a factor of 10^3 .

To provide a thorough cross check, the velocity profiles were determined by several independent methods.

In the first method, velocities were determined by observing the motion of small particles suspended in the fluid. The particles were observed by eye through two grids, to eliminate parallax, and timed by stopwatch. The flow field was illuminated through a slit by collimated light from a slide projector. Velocity observations could therefore be made in one horizontal plane at a time.

The results are shown in Figs. 7, 8, and 9, where velocity U is plotted as a function of the distance normal to the plane of the belts in the region midway between both ends of the test section (see Fig. 3). Clearly, the shear, $S = dU/dy$, is constant in the test section. The flow also appeared to be two-dimensional for a depth of approximately $2/3$ the total depth of the belts. The preceding results were taken with the belts moving at equal and opposite velocities past the test section. Data was also taken with one belt stationary. The velocity profiles for this case are shown in Fig. 10. The profile is no longer linear and, as shown, is clearly a function of Reynolds number. Thus, all further tests and experiments involving drag measurements were made with the belts moving at equal velocities, resulting in a symmetrical linear shear flow in the test section.

It was believed that this lack of linearity for unequal belt speeds was a result of insufficient distance between belt and wall in the return flow section to accommodate the necessary mass flow. With a much wider tank, and a sufficiently large length to width ratio of the test section it was believed that a linear velocity profile with a zero velocity plane

at any desired transverse position in the test section could be generated.

To verify this, Tank 1 was modified considerably after the drag experiments were concluded. The belts were moved much closer together, increasing the test section length to width ratio from 4.65 to 13. This also increased the width of the return channels. A further improvement was made to insure the existence of two-dimensional flow. The working fluid was a light transmission oil which floated on water. The interface was located about midway between the top and bottom edges. In effect, this results in two free surfaces in the oil, thus minimizing the vertical velocity gradient.

Tests were run with one belt completely stationary. The velocity profile was determined by taking a time exposure of white particles suspended on the surface of the oil. The resulting streak lengths are directly proportional to the velocity. Fig. 11 shows two typical photographs. They are negative prints, hence the streaks are black on a white background. Fig. 12 shows the resulting velocity profiles as measured from the photos in Fig. 11. Clearly, the profile is linear for $Re_g \leq 104$. Observation showed that the profile began

to deviate from its linearity at approximately $Re_s = 120$. This critical Reynolds number should increase with increasing length/width ratio of the test section since the deviation is the result of end effects rather than a flow instability.

Since the velocity profile has been verified to be linear for the two limiting cases (zero velocity plane at $y/H = 1/2$ and $y/H = 0$ or 1.0), one may conclude that the zero velocity plane may be transferred to any desired y/H by adjusting the relative speeds of the two belts. This property increases considerably the versatility of this type of shear flow tank.

Another method of determining the velocity profile at the surface consists of observing the deformation of a pattern on the surface of the fluid. This technique is described in section 3.1.4. Fig. 13 shows a series of photographs taken at 5 second intervals. Clearly, the straight line arrangement remains straight, indicating a linear velocity profile.

In order to determine the velocity profile in the vertical plane parallel to the belts another technique was used. A spot of dye was dropped on the surface. Then, with the flow fully developed a small brass sphere was dropped through the dye spot leaving

a thin vertical streak in the flow. (The velocity of fall was much greater than the flow velocity). The dye streak moves with the flow, showing the shape of the velocity profile. A photograph is then taken, from which the velocity profile can easily be determined. Fig. 14 shows the results of such an investigation in Tank 2. The flow is perfectly two dimensional over approximately half the depth of the belt. The velocity drops to 90% of the linear velocity profile at approximately three-fourths the depth of the belt. Naturally, the profile is a function of the lateral distance from the belt, y/H . Fig. 15 shows the approximate area of the test section in which the velocity at a given point is within 10% of the surface velocity at the same lateral distance, y/H . Fig. 16 is a typical photograph used to determine the vertical plane velocity profiles.

The entrance length, i.e., the distance from the ends of the test section required to establish constant shear depends on the Reynolds number, $Re = SH^2/\nu$. By gradually decreasing the viscosity of the fluid it was found that the maximum Reynolds number for constant shear in the test section of Tank 2 was approximately

$$Re_s = \frac{SH^2}{\nu} \approx 400$$

This limiting Reynolds number increases with increasing length to width ratio of the test section, as shown in Chapter 6. An additional study of the breakdown of the linear profile and the gradual transition to turbulence is presented in Chapter 6.

In this apparatus the flow in the return channels between the belts and the tank walls is also approximately a constant shear flow, and the flow only has to adjust to having turned a corner. Thus the region of flow adjustment at the test section is short.

To provide a smooth transition from the test section flow to the bottom of the tank, the distance from the lower edge of the belt to the bottom of the tank is approximately equal to half the width of the belt.

The speed of the belts varied from zero up to about one foot per second. In this range surface waves were always negligible.

3.1.4 Applications - As is often the case, a device invented for one particular use turns out to have direct application to a great variety of problems. Such is the case with the shear flow tank.

The shear flow tank was originally designed for the purpose of measuring the forces on various test models suspended in shear flow from a simple beam balance. It fulfilled this purpose very well, and suggested many further investigations for which the concept of a rectangular test section bounded by moving belts would be useful.

One major area of usefulness is that of flow visualization. Tank 2 was used by Educational Services, Inc. in an educational movie on "Kinematics of Deformation." Using copper bronzing powder forced through silk screen stencils, various patterns were laid on the surface of the test section. As the patterns distorted with the shearing fluid, the effects of shear, strain, and rotation were graphically illustrated. One typical series of pattern deformations is shown in Fig. 13.

Another interesting flow visualization study was carried out by the author. Figs. 17 and 18 show examples of symmetric shear flow about a circular cylinder. With the center of the cylinder at the zero velocity streamline of the undisturbed linear shear flow, the unusual double wake phenomenon appears. Streamlines are visualized by injecting dye from inside

the cylinder into the external flow. Fig. 18 illustrates clearly the existence of four stagnation points on the cylinder.

This type of apparatus can also be used for a variety of studies of hydrodynamic stability. The use of moving boundaries opens the possibility of rendering many phenomena at stationary phase. Examples of possible areas of investigation are : stability of an interface in a shear flow; stability of a shear layer with heat transfer; stability of a shear layer with suspended particles. The above investigations require turning the belt system on its side, so that the belts move in a horizontal plane. Then the upper and lower boundaries of the test section are completely independent, and an interface between two liquids can be maintained in the test section without contamination, as would be the case with only one belt.

3.2 Balance System

Fig. 19 is a schematic of the simple beam balance. A photograph is shown in Fig. 20. All knife edges are ordinary razor blades resting in steel grooves.

The sensitivity weight allows one to adjust the sensitivity of the balance by varying the distance below the main knife edge of the balance center of gravity. The balance has been used to measure forces on models with a resolution of less than 5 dynes.

A small mirror on the balance reflects a narrow beam of light from a fixed source onto a scale approximately 6 feet from the balance. Measurements are made by balancing the model force with known weights in the weight tray, until the light beam indicates the null position (see Fig. 21).

3.3 Measurement of Fluid Characteristics

The viscosity of the test fluid was measured with Cannon-Fenske viscometers (Fig. 22). Since it is a gravity flow device, it gives kinematic viscosity directly. The specific gravity of the fluid was measured with a standard hydrometer. Since the viscosity of aqueous glycerol is very sensitive to temperature, it was necessary to account for the difference in temperature of the fluid in the tank during experimental runs, and of the sample used to measure viscosity. A standard mercury thermometer was used.

The magnitude of the correction was determined from extensive data on the properties of aqueous glycerol found in Ref. (29).

All measurements of model dimensions were made with a micrometer, accurate to one-thousandth of an inch, and machinist's rule, accurate to one-hundredth of an inch.

All time measurements were made with an electric stop clock which read to the nearest hundredth of a second.

CHAPTER IV

DRAG OF A CIRCULAR CYLINDER4.1 Theoretical Considerations

The flow about a two-dimensional circular cylinder presents a very interesting problem because there is no solution to Stokes equations which will satisfy the boundary conditions both at the cylinder and at infinity in an unbounded flow. This illustrates a fundamental difference between the nature of two- and three-dimensional viscous flow. In two-dimensional flow the inertia forces a large distance from the body exert a much greater influence on the total flow field, making it mathematically impossible to obtain a uniform approximation to the total velocity as was the case for three-dimensional flow. Thus for a circular cylinder Oseen's equations must be used at the outset.

Lamb (13) obtained the solution to Oseen flow past a circular cylinder. His solution led to the following formula for the drag per unit length:

$$\frac{D}{L} = \frac{4\pi\mu V}{\frac{1}{2} - \gamma - \ln\left(\frac{Re}{8}\right)} \quad (4.1)$$

where γ is Euler's constant, $\gamma = .5772\dots$. If equation (4.1) is expressed in terms of a viscous drag coefficient, it becomes

$$\alpha = \frac{D}{\mu V L} = \frac{5.46}{\log\left(\frac{7.41}{Re}\right)} \quad (4.2)$$

$$Re = \frac{V \cdot d}{\nu}$$

Experiments have shown that equation (4.2) is valid for $Re \leq .6$ (see Fig. 21).

For analytical solutions at higher Reynolds numbers, one must either employ expansion techniques as described by Proudman and Pearson (7) (see section 2.3) or solve the complete equations by relaxation techniques.

Both Proudman and Pearson, and Kaplun have solved the cylinder flow problem for uniform flow by the Stokes-Oseen expansion method (7, 9). Using this same technique, Bretherton (30) solved for the flow about a circular cylinder in simple shear. Unfortunately his solution is very restrictive, and the special case of uniform flow ($S \rightarrow 0$) cannot be deduced from his solution. Kaplun's solution led to a circular cylinder drag formula as follows:

$$\frac{D}{4\pi\mu V} = \epsilon \left(1 + \sum_{n=2}^{\infty} \alpha_n \epsilon^n \right) \quad (4.3)$$

where $\epsilon = \left[\ln \left(\frac{8}{Re} \right) + \frac{1}{2} - \gamma \right]^{-1}$

$$\alpha_2 \approx -.87$$

No improvement is realized over Lamb's drag equation (4.2) unless several values of α_n are calculated. Kaplun calculated only α_2 and indicated the laborious process by which higher order values of α_n may be calculated.

Several authors have employed numerical methods to obtain solutions for flow about a circular cylinder. A finite difference method was used by Thom (31) to solve the full Navier-Stokes equations for flow past cylinders at $Re = 10$, and this method was used by Kawaguti (32) for flow past cylinders at $Re = 40$. This extremely laborious method was improved by several workers and developed into relaxation methods which were used by Allen and Southwell (10) and applied to the cylinder flow problem at $Re = 0, 1, 10, 100, 1000$ with satisfactory results.

Although it is impossible to satisfy boundary conditions at the cylinder and at infinity using Stokes equations, it is possible to satisfy boundary conditions on boundaries which are only a finite distance from the wall. This fact can be established by rigorous mathematical deduction. However, the following intuitive argument leads to the same conclusion:

Although the inertia terms become comparable to viscous terms only at large distances from the body, they nevertheless dominate the nature of the flow in the two-dimensional case, making it necessary to use Oseen's equations at the outset for flows of infinite extent. However, if a boundary is placed in the flow closer to the cylinder than the region for which inertia terms become significant, then the boundary will, in effect, shield the cylinder from the inertia effects, resulting in a purely viscous, or Stokes flow.

The inertia terms become significant at distances closer and closer to the body as the Reynolds number increases. This is quite apparent in the transition from Stokes flow to boundary layer flow with increasing Reynolds number. Thus, one may regard the flow past a cylinder between boundaries a finite distance away to be Stokes flow for very low Reynolds numbers. Then as Re increases the flow will eventually become Oseen flow when the inertia terms become of importance inside the boundaries. Further increases in Re should considerably minimize the effects of the boundary. Of course, the Reynolds number at which transition from Stokes to Oseen flow takes place is a strong function of the geometry of each particular case.

This transition from Stokes to Oseen flow is most readily apparent in the drag of the body. For a circular cylinder, the Stokes drag will be of the form

$$\frac{D}{\mu VL} = \text{constant} \quad (4.4)$$

where the constant is a function of the wall distance and configuration. At some Reynolds number, equation (4.4) must become invalid as inertia forces take effect, and then one must use Lamb's law,

$$\frac{D}{\mu VL} = \frac{5.46}{\log\left(\frac{7.41}{Re}\right)} \quad (4.2)$$

which indicates an increasing drag coefficient as Re continues to increase. One would expect this transition to occur at lower and lower Reynolds number as the characteristic distance from the cylinder to the walls is increased.

This type of flow behavior was indicated experimentally by White (33) who determined the drag of fine wires falling sidewise in circular containers by measuring their velocity of fall. He had set out to verify Lamb's law of drag at very low Re , but found out that the wall effects completely dominated the flow, resulting in Stokes flow over almost the whole Reynolds

number range for which he tested, even for boundaries 500 diameters away. The highest Reynolds numbers did show a transition to drag coefficients identical with accepted values for infinite flow past a cylinder.

The only theoretical solution of Stokes equations for flow past a two-dimensional circular cylinder in a finite channel was obtained by Bairstow, Cave, and Lang (34). By means of a numerical method of successive approximations, they solved Stokes equations for two-dimensional Poiseuille flow through a channel past a circular cylinder with a diameter equal to one-fifth the width of the channel. This solution gave the drag relationship:

$$\frac{D}{\mu V L} = 7.1 \quad (4.5)$$

where V is the maximum velocity in the channel.

When flow past a cylinder is governed by Stokes equations one may make the same assumptions concerning shear flow as discussed in section 2.3. That is, the drag on a cylinder in simple shear in a finite channel with a relative velocity V at the cylinder is identical to the drag produced by a uniform stream in the same channel moving at a velocity V .

4.2 Experimental Investigation

4.2.1 Introduction - Although Lamb obtained his drag law for Oseen flow past a circular cylinder in 1911, it has only been in comparatively recent years that reliable experimental drag data for cylinders has been produced. One of the earliest investigations was made by Wieselsberger (35) in 1921. Using a wind tunnel, he measured the drag on thin wires in the Re range:

$$4 \leq Re \leq 10^6$$

An earlier study by Relf (36) in 1914 had reached Reynolds numbers only as low as $Re = 10$. The next significant experiments were carried out by White (33) in 1946. His drag data reached $Re = .6$ before wall effects became dominant. This is the threshold of validity of Lamb's law. The first substantial verification of Lamb's law did not come until 1953, when Finn (14) extended drag data to $Re = .06$. He determined the drag by measuring the deflection of fine wires in an air stream. In 1959, a study of cylinder drag was done by Tritton (37) who observed the bending of quartz fibers in the range of $.5 \leq Re \leq 100$.

The present experimental study was undertaken because of the lack of data in the very low Reynolds number range, and the, as yet, undetermined quantitative influence of wall effects for the simple configuration of a circular cylinder between parallel plates. In addition, there has been virtually no experimental data for the drag of a cylinder in shear flow.

The purpose of the following investigation was to determine (1) the magnitude of the drag of a two-dimensional circular cylinder between parallel walls as a function of wall-cylinder geometry and Reynolds number, (2) the nature of the transition from Stokes to Oseen flow, and (3) the influence of shear on the drag.

The experiments were performed using the shear flow tanks and experimental apparatus described in Chapter III.

Drag measurements were made with many different cylinder sizes under a great variety of conditions in order to verify the dimensional similarity relationships as well as to vary the dimensionless parameters over as wide a range as possible. As a further check, drag measurements were made using both Tank 1 and Tank 2 (see Table 1). Table 2 summarizes the range of

parameter variations in the circular cylinder drag experiments. Fig. 24 is a photograph of all the cylinders tested.

4.2.2 Finite Length Effects - It was necessary to evaluate possible end effects of a finite length cylinder in order to interpret the data taken in terms of a two-dimensional, infinite length circular cylinder. Possible corrections arise from three different sources; (1) effect of the submerged end of the cylinder on the two-dimensional drag, (2) surface tension drag, and (3) surface wave drag.

In order to evaluate these corrections, drag measurements were made on cylinders of the same diameter, but with different lengths. Figures 25 and 26 illustrate the results. Since the drag coefficient remained independent of the length to diameter ratio (aspect ratio) for both diameters tested, (within the accuracy of the measurements) it was concluded that all end effects were negligibly small, since for all additional tests, $L/d \geq 28$, and end effects will naturally decrease with increasing L/d .

4.2.3 Results - Figures 27 and 28 plot drag coefficient, α , versus Reynolds number, Vd/ν , for various values of the wall nearness ratio, d/H . This family of data was taken with the cylinder axis located at $y/H = 1/3$. This same qualitative variation is obtained for all values of y/H (until the cylinder contacts the wall).

It is clear that at low Reynolds numbers the results indicate the existence of Stokes flow,

$$\frac{D}{\mu VL} = \text{constant}$$

With increasing Re , the drag curves eventually merge with Lamb's curve and the accepted drag curves for infinite extent flow. All of the drag data were taken in shear flow. This has no effect in the Stokes regime, as explained in Section 2.3. It appears also that in the shear range of this experiment, the shear has little or no effect during the initial stage of Oseen flow either. As d/H increases, both the Stokes flow drag coefficient and the Reynolds number of transition from Stokes flow to Oseen flow increase.

Fig. 27 indicates that in the Stokes flow regime, the viscous drag coefficient is a function only of the

wall nearness ratio, d/h . Fig. 29 is a plot of the Stokes flow drag coefficient as a function of d/H . These experimental points are described quite well by an empirical formula of the form

$$\alpha_{\frac{y}{H} = \frac{1}{3}} = \frac{D}{\mu VL} = \frac{6.3}{\log \frac{H}{d}} \quad (4.6)$$

where V is the undisturbed relative velocity at the cylinder axis. Equation 4.6 is valid for a cylinder distance of $y = (1/3)H$ from the wall. In order to determine the drag of a cylinder midway between parallel walls, it was necessary to measure the drag at several values of y/H and extrapolate to $y/H = 1/2$, since the velocity was zero at the center of the test section. The belts were always run at equal and opposite velocity past the test section to insure perfectly linear shear flow.

Such an extrapolation led to the empirical formula

$$\alpha_{\frac{y}{H} = \frac{1}{2}} = \frac{5.9}{\log \frac{H}{d}} \quad (4.7)$$

Fig. 30 shows the variation of α as a function of y/H .

The experimental scatter of data makes it difficult to give a quantitative formula for the drag variation with lateral distance. However, one may conclude that the Stokes drag of a circular cylinder between parallel plates is given empirically by the formula

$$\alpha \log \frac{H}{d} = K\left(\frac{y}{H}\right) \quad (4.8)$$

where $K(y/H)$ increases monotonically from $K(1/2) = 5.9$ to $K(0) = \infty$. Note that K increases only about 13% as y/H varies from $1/2$ to $1/6$.

Thus it is clear that there are two distinct drag laws for circular cylinders between parallel plates; Equation (4.8); and Lamb's law, equation (4.2).

For low Reynolds numbers (4.8) applies; but with increasing Re , inertia forces became significant, "shielding" the cylinder from the effect of the walls and the drag is the same as that in an infinite fluid. Then (4.2) is valid (if $Re \leq 6$). To determine the approximate region of transition, (4.8) and (4.2) may be solved simultaneously for the transition Reynolds number, Re_T .

$$\left. \begin{aligned} \alpha_T &= \frac{K}{\log \frac{H}{d}} \\ \alpha_T &= \frac{5.46}{\log \left(\frac{7.41}{Re_T} \right)} \end{aligned} \right\} \quad (4.9)$$

$$\frac{\log 7.41 - \log Re_T}{5.46} = \frac{\log \frac{H}{d}}{K}$$

$$\log Re_T = \frac{5.46}{K} \log \frac{d}{H} + \log 7.41$$

$$Re_T = 7.41 \left(\frac{d}{H} \right)^{\frac{5.46}{K}} \quad (4.10)$$

As Fig. 27 shows, the actual Reynolds number at which Lamb's law starts to become invalid may be from 25% to 50% higher than Re_T given by (4.10) since the transition takes place gradually over a region in which Re may vary by a factor of 2.

White (33) made a few measurements of the drag on cylinders falling midway between parallel plates. However, his data had an unusually high amount of scatter and some questionable end corrections were also applied. Taking the mean value of his data which was all in the Stokes regime, he found that $K(1/2) = 6.4$. This compares with $K(1/2) = 5.9$ found in this study which is believed to be more accurate because of the reduced scatter and direct force measuring technique.

The drag coefficient found by Bairstow, Cave, and Lang (34) is given as

$$\alpha = 7.1, \quad \frac{d}{H} = \frac{1}{5} \quad (4.5)$$

In terms of equation 4.8 this gives a value of $K(1/2) = .50$. However, this is based on the maximum velocity in the channel. Thus, it appears that a cylinder moving at velocity V through a channel with the fluid at rest experiences the same drag as a cylinder at rest in the same channel with fluid flowing past in a parabolic profile with a maximum velocity of $1.18V$. This may be subject to a further correction since it assumes that equation (4.7) can be extrapolated to $d/H = .20$. The highest value verified in this study was $d/H = .104$.

One factor has not been mentioned yet. There is probably a drag contribution from the walls due to asymmetric boundaries when $\frac{y}{H} \neq \frac{1}{2}$, even though the undisturbed relative velocity at the cylinder axis is zero. One would expect this drag to be negligible compared to the drag due to the undisturbed relative velocity V as long as

$$\left. \begin{array}{l} \frac{Sd}{V} \ll 1 \\ \text{and } \frac{y}{d} \gg 1, \quad \frac{y}{H} < \frac{1}{2} \end{array} \right\} \quad (4.11)$$

Since the conditions of equations 4.11 were met for all the tests, the drag due to asymmetry of the boundaries was neglected.

There is another interesting characteristic of this type of flow which should be noted. In the Stokes flow regime, the drag is independent of the Reynolds number, as shown in Figure 27, and for Stokes flow between parallel walls, the drag on a circular cylinder is

$$D = \text{constant} \times \mu VL \quad (4.12)$$

Clearly, the drag is independent of cylinder diameter, as long as the wall nearness ratio d/h remains fixed, since the constant in equation (4.12) is a function of d/h .

Although seemingly paradoxical, this phenomenon may be explained quite simply in physical terms. The drag due to viscosity is the result of a shearing force at the surface of the cylinder. But as d increases H must increase proportionately. Thus the distances over which velocity gradients must take place are increased, and the shearing rates then decrease just the right amount to compensate for the increased surface area. This same line of reasoning also accounts for the constancy of the drag due to pressure. The net result is that for constant μ , V and d/h , the diameter of a cylinder may be increased indefinitely without changing the drag per unit length, as long as the Reynolds number does not exceed the limits for Stokes flow.

CHAPTER V

DRAG OF A SPHERE5.1 Introduction

Unlike the case of drag of a circular cylinder, there has been a great deal of experimental data on sphere drag for many years. Reference (39) gives a comprehensive bibliography of experimental sphere drag studies. All previous data has been for the case of uniform flow past a sphere. However, the motion of spheres in shearing flows has become of considerable interest in recent years. Several workers have studied phenomena associated with neutrally bouyant spheres in laminar pipe flow. But neutrally bouyant particles are certainly the exception rather than the rule. Hence, it is felt that some basic experimental methods should be developed for the study of forces on particles in simple shear flow. Thus one can obtain data which may shed light on some of the more complex phenomena associated with non-linear velocity profiles and unsymmetrical boundary conditions.

This chapter describes the technique used to measure the drag of a stationary sphere in simple shear flow. Results of measurements taken over the range

$$3.8 \times 10^{-2} \leq Re \leq 2.3$$

are presented also. In this range there is a known theoretical solution (see Chapter II); thus one can assess interference effects accurately.

5.2 Experimental Apparatus

Experiments were performed using the shear flow apparatus described in Chapter III. The test spheres were mounted on thin circular cylinders which were suspended from the beam balance (see Fig. 20). During all tests the spheres were located at a distance $y = (1/3)H$ from the test section wall (belt), so that they would experience a relative velocity. A wide variety of model dimensions were used to accurately confirm the results. The range of test conditions are summarized in Table 3. Fig. 31 defines the model dimensions. A photograph of all the sphere models tested is shown in Fig. 32.

5.3 Results

The results of the experiments are shown in Figures 33, 34, and 35. The drag values were deduced in the following manner. First the total drag on the sphere and cylinder was measured. Then the drag of a cylinder alone, of the same dimensions as the cylinder mount, was subtracted from the total drag. The cylinder drag was obtained from the data of Chapter IV. The remaining drag was that of the sphere plus interference drag. (For details of this calculation procedure, see Appendix A.) This remainder is plotted in the above mentioned graphs. These results indicate that within experimental accuracy, the drag coefficient of a sphere is independent of the mounting geometry in the ranges tested. Furthermore, this drag coefficient is equal to the Stokes drag coefficient for uniform flow of the same mean velocity, as predicted by the theoretical analysis of Chapter II. This data provides an excellent experimental verification of the linearity of Stokes flow in both pressure and velocity.

Since the interference drag appears to be negligible, this technique provides an excellent method for similar studies in the higher Reynolds number range.

Interference effects would be expected to even decrease as Re increases, since the extent of perturbations are at a maximum in Stokes flow.

All of the drag data is for a non-rotating sphere. Several attempts were made to construct a mounting on which the sphere could rotate freely in the shear flow. However, all attempts proved unsuccessful except with the sphere at zero mean velocity. The friction due to the drag forcing the sphere against the bearing surface was too great compared to the extremely small moment due to shear to allow the sphere to rotate freely.

5.4 Analysis of Interference Effects

Brenner (38) gives a method of estimating the effects of the parallel walls and the free surface on the Stokes drag coefficient of a sphere. Brenner shows that for a spherical particle, the effect of the presence of a boundary can be represented by an equation of the form

$$\frac{D}{6\pi\mu aV} = \frac{1}{1 - c\frac{a}{h} + O\left(\frac{a}{h}\right)^3} \quad (5.1)$$

where D is the drag in the presence of the boundary, a/h is the ratio of sphere radius to boundary proximity, and c is a constant which is a function of the particular sphere-boundary geometry.

For a sphere falling midway between two infinite, plane, parallel walls, and moving parallel to them,

$$c = 1.004 \quad (5.2)$$

For the largest sphere, $a/h = .1035$. Then

$$\frac{D}{6\pi\mu aV} = \frac{1}{1 - (1.004)(.1035)} = 1.115 \quad (5.3)$$

However, for a sphere moving parallel to an infinite free surface,

$$c = -\frac{3}{8}$$

The largest sphere was about 8 radii from the surface, giving $a/h = .125$. For this case

$$\frac{D}{6\pi\mu aV} = \frac{1}{1 + \frac{3}{8}(.125)} = .955 \quad (5.4)$$

Hence, the walls produce an 11.5% increase in drag, and the free surface causes 4.5% decrease. Thus for the worst case, we can expect a 7% increase in drag. But this is further offset by the fact that the flow field about the sphere would be expected to decrease

the drag of the supporting cylinder below the two-dimensional value. Hence, by subtracting the full two-dimensional drag of the cylinder from the total drag, one obtains slightly less than the actual drag experienced by the cylinder. This deficit is about 5% to 10%. This places the final result within 5% of the Stokes drag of a cylinder in an infinite fluid, if the sum of all other interference effects are of this order of magnitude or less. This deviation is also less than the expected experimental error (see Appendix B). This analysis is substantiated by the results which show that the mean value of all the data taken for spheres is within $\pm 5\%$ of the Stokes drag.

5.5 Free Rotation of a Sphere in Shear Flow

A body immersed in a shear flow will experience a moment causing it to rotate. In a theoretical analysis, Vand (21) has shown that a sphere immersed in a linear shear flow with a constant shear S will rotate under steady state conditions with an angular velocity ω such that

$$|\omega| = \frac{1}{2} S \quad (5.5)$$

if Stokes equations are valid. That is

$$Re_s = \frac{\rho d^2}{\eta} \ll 1$$

Previous investigators (24) have verified equation (5.5) at Reynolds numbers below 10^{-6} . The present investigation extended the Reynolds number of validity of equation (5.5) to $Re_s = 1.0$.

Measurements were made by suspending a neutrally bouyant plastic sphere in the shear flow. The rate of shear of the flow was determined by measuring the belt speed by stopwatch, and the rate of rotation of the sphere was determined by timing the period of rotation by stopwatch also.

The results are plotted in Fig. 36. Clearly, the ratio $\omega/\dot{\gamma}$ remains constant at $1/2$, up to the highest Reynolds number tested, $Re_s = 1.0$, within experimental accuracy.

CHAPTER VI

INVESTIGATION OF SHEAR FLOW CHARACTERISTICS6.1 Introduction

The purpose of this investigation was to explore the capabilities and limitations of the shear flow tank developed as a part of this thesis. In addition, some preliminary data was taken on the stability characteristics of rectilinear Couette flow.

6.2 Experiments6.2.1 Effect of Test Section Length-Width Ratio -

As one would expect, the length to width ratio L/H has a significant effect on the maximum Reynolds number for which uniform shear flow can be obtained. To demonstrate this, the belts were moved closer together in Tank 1 and additional velocity profile measurements were made. Another improvement was the use of oil floating on water as a flow medium. Because of the large difference in viscosity between oil and water, the interface (located about midway between the top and bottom of the belts) acted essentially as a second

free surface. This resulted in a much improved two-dimensionality of the flow. Measurements were made with $A/H = 13$.

The first tests were made with one belt stationary. The results, reported in Chapter III, indicate clearly the improvement: for $A/H = 4.65$, the $Re_g = 76$, the velocity profile was obviously nonlinear (Fig. 10). But with $A/H = 13$, the velocity profile with one belt stationary was linear for Reynolds numbers as high as $Re_g = 120$ (Fig. 12).

Tests were also conducted with both belts moving at equal and opposite velocities. The velocity profile measurements were made by taking a time exposure of small white plastic particles suspended on the surface of the oil. The resulting streak lengths are directly proportional to the velocity. The photographs were taken on Polaroid transparent film (Type 146L) which gave positive transparencies from which negative prints were made. Typical photographs are shown in Figures 37 and 38. The velocity profiles as determined from these prints are shown in Figures 39 and 40. Hence a linear velocity profile is maintained for $Re_g = 721$ and $A/H = 13$. Observations made in Tank 2 indicated that the profile began to deviate from linearity

at $Re_g \approx 400$ for $\Lambda/H = 6$. This illustrates clearly the strong influence of Λ/H on the maximum Re_g for the existence of a linear velocity profile in the test section.

6.2.2 Instability of Couette Flow - To investigate the stability characteristics of laminar rectilinear Couette flow, flow pictures were taken for progressively increasing Reynolds number. In the following study, the belts were always moved at equal and opposite velocities past the test section.

As shown in Fig. 40, the flow remains laminar with a linear velocity profile up to $Re_g = 721$. Fig. 41a shows the flow pattern for $Re_g = 885$. In this photo, the first slight deviations from rectilinear flow appear. The zero velocity plane also shows deviations from its normal position at $y/H = 1/2$. At $Re_g = 1260$, (Fig. 41b) the flow continues to remain basically laminar, but the same general deviations noticed in Fig. 41a continue to exist.

The preceding pictures were taken with oil as a flow medium. The following flow pictures at higher Re_g were taken using water as a flow medium. The change was necessitated because the increased belt

velocity required for higher Re_g resulted in objectionable waves at the free surface and particularly at the oil-water interface. By using water, with a much lower viscosity, correspondingly lower belt velocities could be utilized thus avoiding surface waves. With water, aluminum particles sprinkled on the surface were used for flow visualization. Unfortunately, with water there was a lower limit to the belt velocity. This was the result of the fact that surface tension causes the particles to gradually agglomerate. Hence, the flow velocity must be an order of magnitude greater than the drift velocity of the particles, and the flow phenomena must occur before the particles have time to agglomerate and obscure the flow pattern. In addition, the slower the flow velocity the more difficult it was to obtain enough photographic contrast because of the excessively long exposure time required.

Hence, using water for the flow medium, the lowest Re_g was 13,500 shown in Fig. 42a. Here the flow pattern has changed drastically from that at $Re_g = 1260$. The velocity profile is obviously non-linear, and the flow appears to be dominated by a series of vortices located approximately in the center of the channel.

Since several streak lines intersect at finite angles, the flow now is obviously unsteady. Visual observation showed that the vortices were continuously generated and dissipated after the flow was established. This same basic pattern continued to exist for increasing Re_g up to $Re_g = 32,000$ as shown in Figures 42 and 43. Visual observation indicated that the flow had not yet reached fully developed turbulence at $Re_g = 32,000$. The very short wave length oscillations are due to surface waves rather than a flow instability. Thus the actual flow is somewhat smoother than indicated by the photographs.

There were two main characteristics which yielded quantitative data: wavelength and amplitude of the primary disturbances. The wavelength, in terms of channel width H , is defined as the distance between the centers of adjacent vortices. Using the flow photographs, the wavelength was measured and plotted as a function of Re_g in Fig. 44a. The wave number, $\delta = \frac{2\pi}{\lambda}$, is plotted in Fig. 44b. In spite of the scatter, which is to be expected, a definite trend is established.

The amplitude is defined as the maximum lateral width of a band in the center of the channel within which the fluid is entrained in the circulatory motion of the vortices. Outside of this "amplitude band", the fluid continues to maintain a mean rectilinear motion. Table 4 shows the approximate amplitude of the main disturbances for various Reynolds numbers. Over the range investigated, the amplitude appears to remain approximately constant at $.4H$.

6.3 Discussion

Rectilinear Couette flow is the most simple case of laminar viscous flow. Thus one might expect a simple stability problem also. However, no conclusive answer has yet been reached concerning this problem. Many authors have dealt with this problem, but all investigations indicate that the flow is always stable with respect to small disturbances (42, 43, 44, 45). Although there have been very few experimental investigations of the problem, it is an accepted fact that rectilinear Couette flow does become unstable at higher Reynolds numbers (41). Of course, the problem of finite disturbances has not been solved, and Lin (46) points out that to show that the motion

is stable with respect to all modes of infinitesimal disturbances still remains to be done. Orr (47) has shown theoretically that rectilinear Couette flow must be stable for $Re_g < 88.6$. Present data verifies that the flow remains laminar for Re_g considerably higher than this value.

One must now consider the question of the validity of the data reported in section 6.2.2. The scarcity of experimental data in this area makes this a difficult task.

Consider first the critical Reynolds number at which transition to turbulence takes place. The present study indicates that transition begins somewhere in the range $10^3 < Re_g < 10^4$. Experimental data available from Reichardt (28) records that transition occurred in his apparatus at $Re_g = 3,000$. Fig. 41 shows deviations from rectilinear flow at a Reynolds number as low as $Re_g = 885$. This points out the important question of what is the influence of the finite length of the test section. Is the stable linear velocity profile deformed initially by the end effects to an unstable profile which then becomes turbulent? Or does the flow at each end

become ^{un}stable first, and then propagate unstable disturbances into the test section region? Disturbances generated by the belts themselves may also have considerable influence in the transition process. This was pointed out by Reichardt in a later work (41) in which he constructed a more refined apparatus. Unfortunately, all tests in the new apparatus were carried out at Reynolds numbers where fully turbulent flow was already established. One must also recognize that there is a vertical velocity gradient which must presumably become unstable eventually. If this occurs before instability of the two-dimensional Couette flow, it could significantly affect the transition process.

All of these factors may influence the form of the first unstable mode, wavelength, and amplitude. Unfortunately, Reichardt did not report any observations of the process of transition to turbulence in his apparatus. He was concerned primarily with the shape of the velocity profile. As a partial check on the influence of the length to width ratio, the flow patterns in Figures 42 and 43 were taken at two different values of L/H . In Figures 42b and 43b, $L/H = 7.4$, and

in Figures 42a and 43a, $\lambda/H = 13$. This change has no apparent effect on the basic flow pattern, the wavelength trend, nor the amplitude. Of course, this evidence cannot be regarded as conclusive.

A recent experimental study by Thomas (51) has yielded some very encouraging results. Using equipment of a much smaller scale ($H = .44$ in.) and a high length to width ratio ($\lambda/H = 26$), Thomas investigated the stability characteristics of Couette flow. He found that the first detectable deviations from a linear profile occurred at $Re_s = 1,410$. The vortices first became visible at approximately $Re_s = 3,400$. Wavelength measurements gave the following results: At $Re_s = 9,240$, $\lambda/H = 1.4$. At $Re_s = 17,750$, $\lambda/H = 1.87$. The close agreement of this data with the results both of the present study and the work of Reichardt helps to establish the validity of this type of experimental approach to the problem of Couette flow stability.

Now consider the possible relationship of the present experimental data to various theoretical studies. An interesting comparison may be made between the flow patterns evident in Figures 42 and 43 and the results of an investigation by Hopf (43).

Using the method of small disturbances, Hopf showed that there are three primary types of oscillations in a viscous fluid at rest. The fundamental mode exhibits a mode shape as shown in Fig. 45a. The higher harmonics correspond to multiple subdivisions of the fluid. Type 2 oscillations are generally of the same character as Type 1, but the mode shapes are distorted by the primary shear flow velocities, as shown in Fig. 45b. Hopf showed that all the disturbances are stable, but have the least damping midway between the walls. Thus the fundamental mode will persist over the higher harmonics. Type 3 oscillations tend to persist near the wall and behave independently in their respective stream layers. They are characteristic of higher Reynolds numbers and are closely related to the eventually fully developed turbulence. The higher harmonics appear closer to the plane midway between the walls and are highly damped, thus would not be as readily apparent in a flow picture as Types 1 and 2. The similarity between the mode shapes of Types 1 and 2 and the flow patterns of Figures 42 and 43 is apparent.

Now consider whether the wavelengths reported in Fig. 44 are consistent with data from related investigations. For the case of plane Poiseuille motion between plates a distance H apart, Shen (48) found the highest value of a neutrally stable wave number to be $\gamma H = 2.28$. This corresponds with a wavelength of

$$\lambda = \frac{2\pi H}{2.28} = 2.78 H$$

For the case of a Blasius profile, Shen found the largest neutrally stable wave number to be $\gamma \delta^* = .41$, where δ^* is the displacement thickness. This corresponds to a wavelength of

$$\lambda = \frac{2\pi \delta^*}{.41} = 15.3 \delta^* \approx 5 \delta$$

where δ is the boundary layer thickness. Note the difference between the symmetrical shear layer and the boundary layer type. Another comparison is gleaned from the work of Lessen (49) who studied the stability of the laminar viscous layer between parallel streams. Some of his results are shown in Fig. 46, where the wave number γ is plotted as a function of Reynolds number for constant amplification rate. Here δ is

the width of the viscous boundary layer. The values of δ range in the neighborhood of .2 to .5, and the unstable Reynolds numbers are quite low. But the most interesting result is the shape of the curves in Fig. 46 in comparison to the curve in Fig. 44 for Couette flow. They bear a definite resemblance to one another. There is a difference which should be noted, however. Lessen's curves tend to an asymptotic value of δ as $Re \rightarrow \infty$. The present data does not indicate the presence of an asymptote, although experiments must be performed in a wider parameter range to be certain. Lessen's data is for small disturbances. Also, the presence of the walls in Couette flow may have a significant effect. Thus one cannot expect more than a rough qualitative agreement between Lessen's theory and this experimental data. Nevertheless, this type of flow bears perhaps the greatest resemblance to Couette flow. Furthermore, the somewhat lower values of δ found by Lessen might be expected if one considers the following: The results of Hopf indicate that instabilities will first occur in the center of the channel. The finite disturbances alter the velocity profile in the center causing an

inflection point to appear, which further enhances the instability. However, this inflection point region will initially extend only a short distance from the center. Thus a typical length should more properly be somewhat less than H . This adjustment would result in a closer agreement of the present results with the data of Lessen.

As stated previously, these results are not entirely conclusive. There is still need for extensive further experiments with more refined and versatile apparatus. The following improvements and extensions are suggested by the author: Conclusive experiments will require much higher values of Λ/H . With a high Λ/H , the stability characteristics will be independent of the ratio of the two belt speeds if the flow is successfully isolated from extraneous influences. This must be further verified by changing the inlet geometry at each end in a variety of ways. Every effort must be made to limit extraneous flow disturbances to an absolute minimum. This will require the belt to always travel against a stabilizing surface to eliminate belt vibrations. It is felt that this may considerably increase the critical

Reynolds number of transition because of the inherent stability of Couette flow with respect to small disturbances. The apparatus must also be large enough to obtain high Reynolds numbers with relatively low belt speeds in order to avoid the effects of surface waves. Improved photographic and measurement techniques must also be developed. Present technique allows one to investigate only the flow at the surface of the fluid. In view of the possible importance of three-dimensional disturbances, improved visualization techniques would be very useful.

CHAPTER VII

DISCUSSION AND CONCLUSIONS7.1 Experimental Apparatus

A method of developing a laminar, rectilinear Couette flow has been successfully developed. A two-dimensional, linear velocity profile was obtained for Reynolds numbers up to $Re_g = 721$. The shear flow tank was especially useful in studying low Reynolds number phenomena. Studies of Couette flow stability were limited somewhat by the physical characteristics of the tank. However, the experiments suggested several modifications which should improve reliability considerably.

Although a linear velocity profile was obtained for a test section length-width ratio as low as $L/H = 4.65$, it was found that in order to avoid end effects at high Reynolds numbers, L/H should be at least 20, or higher. This makes it possible to maintain pure Couette flow with one belt stationary up to the Reynolds number of instability. If the test section

is to be wide enough to afford adequate visual and physical access, a rather long test section and correspondingly long belts will be required. Hence, the following suggestions are offered. To avoid the excessive drag of pulling a belt past a flat plate, the stabilizing surfaces should be open grids, rather than flat plates with just a few holes. Furthermore, to avoid disturbances arising from belt vibrations, the belt should always move parallel to a stabilizing surface. The major problems encountered with the belts were belt slippage and a tendency for the belts to ride up or down on the rollers. Both of these problems can be solved by using a notched belt and sprocket rollers.

7.2 Cylinder Drag, Sphere Drag, and Stability

The existence of a Stokes flow regime for flow past a two-dimensional circular cylinder in a finite channel was conclusively demonstrated. For sufficiently low Reynolds number the viscous drag coefficient became constant, independent of Reynolds number. In the Stokes flow regime it was found that the drag could be given empirically by the following formula:

$$\alpha \log \frac{H}{d} = K \left(\frac{\nu}{H} \right)$$

$$\alpha = \frac{K \left(\frac{y}{H} \right)}{\log \frac{H}{d}} \quad (7.1)$$

where K is an empirically determined constant which varies from $K(1/2) = 5.9$ to $K(1/3) = 6.3$, and $K(0) = \infty$. This formula applies to a cylinder moving between parallel walls in which the fluid is at rest. It was also shown that the drag was unchanged if a symmetrical constant shear is superposed on the uniform flow. This is a natural result of the linearity of Stokes equations in velocity and pressure. With increasing Re , there is a gradual transition from Stokes flow to Oseen flow, as demonstrated by the transition of the drag from equation 7.1 to Lamb's law (equation 4.2). This occurs as the inertia forces become significant closer and closer to the cylinder, eventually shielding the cylinder from the effect of the walls. In the range of parameters tested, the shear rate had no apparent effect on the drag.

Extensive drag measurements on a sphere in shearing Stokes flow were also made. The linearity of Stokes flow was experimentally verified. It was also demonstrated that the interference drag between

the sphere and mounting cylinder, as well as all other interference effects were negligible. Thus the techniques developed in this study were established as a practical method for investigating a much wider variety of problems involving three-dimensional bodies. It is hoped that a more sensitive force measuring technique will eventually make it possible to investigate transverse forces on bodies in a shear flow at low Reynolds number.

The rotation rate of a free sphere in a uniform shear flow was measured. It was found that the sphere rotates at a rate equal to one-half the vorticity, or shear rate S , as predicted theoretically by Vand, up to the highest Reynolds number tested, $Re_s = 1.0$.

The high Reynolds number characteristics of rectilinear Couette flow were investigated. It was found that the laminar velocity profile first begins to deviate from linearity at approximately $Re_s = 10^3$. Vortices appear midway between the belts at approximately $Re_s = 3,000$. This is the value at which Reichardt observed the flow in his apparatus to become "turbulent." Observation showed that as the Reynolds number continued to increase, the flow was dominated by a system of

vortices midway between the belts whose wavelength gradually decreased. No trend toward a definite asymptote was observed. The flow became more irregular at higher Reynolds numbers, but a definite vortex system could still be observed at $Re_g = 32,000$. Although generally corroborating evidence was obtained by Thomas (51), much more experimentation remains to be done in this area. Detailed recommendations are offered in Chapter VI.

It is believed that the development of the shear flow tank and the accompanying experimental techniques have opened a wide area for investigation of various phenomena associated with shear flows. The fundamental shear flow tank concept can be applied to a great variety of stability problems as well as many more investigations such as fluid dynamic forces, particle motion, and even heat transfer problems in shear flows.

APPENDIX A

DETAILS OF CALCULATION OF EXPERIMENTAL DRAGA.1 Circular Cylinder Drag

Experiments were conducted with the cylinders mounted in the Jacob's chuck of the beam balance, Fig. 20, and extending into the flow tank perpendicular to the free surface. The drag is measured by balancing the drag moment about the main knife edge with a known weight w in the balance tray. It is assumed that the drag per unit length is constant over the total submerged length of the cylinder. Thus the equivalent moment arm is the distance from the main knife edge to the middle of the submerged portion of the cylinder. If this distance is A , and the distance from the main knife edge to the balance tray knife edge is B , then the drag on the cylinder is

$$D = w \frac{B}{A} \quad (A.1)$$

The assumption of constant drag distribution over the submerged length is verified by testing several lengths of the same diameter. If the drag is two-dimensional, the drag per unit length will remain unchanged, as verified in Figures 25 and 26.

A.2 Sphere Drag

The geometry of the sphere and mounting cylinder are shown in Figure 31. The total drag of the sphere and cylinder is measured in the manner described in the previous section concerning cylinders. Let w be the known balancing weight, A is the distance from the center of the submerged cylinder to the main knife edge, and B is balance tray moment arm.

Now the balance weight W_c needed to balance the drag of the cylinder alone is

$$W_c = \alpha \mu V L \frac{A}{B} \quad (\text{A.2})$$

where α is the two-dimensional drag coefficient of the cylinder, L is the submerged cylinder length.

Now if C is the distance from the center of the sphere to the main knife edge, then the sphere drag plus all interference drag is given by

$$D = (w - W_c) \frac{B}{C} \quad (\text{A.3})$$

APPENDIX B

ACCURACY OF EXPERIMENTAL DATAB.1 Accuracy of Individual Measurements

This section tabulates the maximum error of each contributing measurement with appropriate comments on experimental technique and the method of estimating the error.

Drag-D

The drag was measured with a simple beam balance. Experience showed that it could be balanced within $\pm 5\%$ at the extreme lower values of the drag measured. Since the absolute error tended to remain constant, this value decreased considerably for the large majority of the experiments, averaging approximately $\pm 2\%$.

Relative Velocity - V

The relative velocity at the axis of the cylinder was determined by measuring the velocity of the belt U_B and applying the formula

$$V = U_B \left(1 - 2 \frac{Y}{H}\right) \quad (\text{B.1})$$

The velocity of the belt was determined by measuring the interval of time required for a mark on the belt to travel between two points a known distance apart. The starting and stopping of the stopwatch introduced a maximum error of 0.1 seconds. Since in all but a very few cases the time interval was greater than 10 seconds (most were 20 to 60 seconds in length), the maximum error in U_B is $\pm 1\%$.

The maximum error in position, y/H , was .01 in., corresponding to a maximum error in $(1-2 y/H)$ of $\pm 1\%$.

Thus the total maximum error in V is $\pm 2\%$.

Kinematic Viscosity - ν

The kinematic viscosity was measured with Cannon-Fenske viscometers which have an accuracy of $\pm .2\%$. However, it was necessary to correct for the difference in temperature of the fluid sample in the viscometer and the tank fluid temperature. This introduced a possible error of approximately $\pm 2\%$. The viscosity was obtained with the help of conversion tables in Reference 29 from the kinematic viscosity, and thus has approximately the same error as ν .

Cylinder Length - L

Length measurements were made with a machinist's rule and calipers. They are accurate within ± 0.01 in. Thus, the maximum length error is $\pm 0.5\%$; with most cylinders this error is considerably less.

Diameter - d

Cylinder and sphere diameters were measured with a micrometer with an accuracy of ± 0.0001 in. Thus the maximum error for cylinders is $\pm 0.8\%$, and for spheres, $\pm 0.04\%$.

Density - ρ

To obtain density, the specific gravity was measured with a hydrometer with an accuracy of $\pm 0.25\%$.

B.2 Accuracy of Final Results

The drag coefficient α of a circular cylinder is

$$\alpha = \frac{D}{\mu V L} \quad (\text{B.2})$$

Thus the maximum expected error in α is found to be $\pm 6.5\%$. Typical results shown in Fig. 27 indicate an experimental scatter well within this 13% band of possible scatter, with the great majority of the data lying within a scatter band of about 5%.

The drag coefficient C_D of a sphere is

$$C_D = \frac{D}{\frac{1}{2} \rho V^2 \pi (d/2)^2} \quad (\text{B.3})$$

Hence, C_D may be expected to have a deviation of $\pm 6.3\%$, or to exhibit scatter over a band of approximately 12.6%. Figures 33, 34, and 35 show all experimental results fall within these limits.

The Reynolds number is

$$Re = \frac{V d}{\nu}$$

and will have a maximum error of $\pm 4.8\%$.

REFERENCES

1. Stokes, G.G., "On the Effect of the Internal Friction of Fluids on the Motion of Pendulums", Camb. Phil. Trans., V. 9, No. 8, 1851.
2. Hoglund, R.F., "Recent Advances in Gas-Particle Nozzle Flows," ARS Journal, V.32, No. 5, May 1962.
3. Prandtl, L., "Über Flüssigkeitsbewegung bei sehr kleiner Reibung," Proc. of Third Intern. Math Kongr., Heidelberg, 1904; NACA TM 452, 1928.
4. Oseen, C.W., "Über die Stokes'sche Formel und über eine verwandte Aufgabe in der Hydrodynamik," Arkiv für matematik, astronomi och fysik, V.6, No. 29, 1910.
5. Oseen, C.W., Neuere Methoden und Ergebnisse in der Hydrodynamik, Leipzig: Akademische Verlagsgesellschaft, 1927.
6. Lagerstrom, P.A., and Cole, J.D., "Examples Illustrating Expansion Procedures for the Navier-Stokes Equations," Jour. Rational Mech. Anal., V.4, p. 817, (1955).

7. Proudman, I. and Pearson, J., "Expansions at Small Reynolds Numbers for the Flow Past a Sphere and a Circular Cylinder," Jour. Fluid Mech., V.2, P. 237, (1957).
8. Kaplun, S., and Lagerstrom, P.A., "Asymptotic Expansions of Navier-Stokes Solutions for Small Reynolds Numbers," Jour. Rational Mech. Anal., V.6, p. 585, (1957).
9. Kaplun, S., "Low Reynolds Number Flow Past a Circular Cylinder," IX International Congress of Applied Mechanics, Brussels, Sept. 1956.
10. Allen, D.N., and Southwell, R.V., "Relaxation Methods Applied to Determine the Motion, in Two Dimensions, of a Viscous Fluid Past a Fixed Cylinder," Q. Jour. Mech. and App. Math., V.8, p. 129, (1955).
11. Percy, T., and McHugh, B., "Calculation of Viscous Flow Around Spheres at Low Reynolds Numbers," Phil. Mag., V.46, p. 783, (1955).
12. Jenson, V.G., "Viscous Flow Round a Sphere at Low Reynolds Numbers (< 40)," Proc. Roy. Soc., V. A-249, p. 346, (1959).

13. Lamb. H., Hydrodynamics, 6th Ed., Dover Publications, N.Y., 1945.
14. Finn, R.K., "Determination of the Drag on a Cylinder at Low Reynolds Numbers," Jour. Appl. Physics, V.24, No. 6, 1953.
15. Vidal, R.J., "Aerodynamic Processes in the Downwash Impingement Problem," IAS Paper No. 62-36, 1962.
16. Murray, J.O., "Non-uniform Shear Flow Past Cylinders," Q.J. Mech. and App. Math., V.10, February 1957.
17. Mitchell, A.R., and Murray J.O., "Flows with Variable Shear past Circular Cylinders," Q.J. Mech. and App. Math., V. 10, Feb. 1957.
18. Edmunds, D.E., "The Moving Airfoil in Shear Flow in Neighborhood of a Plane Boundary," Q.J. Mech. and App. Math., V.10, 1957.
19. Schlichting, H., Boundary Layer Theory, 4th Edition, McGraw Hill Book Co., Inc., New York. 1960.
20. Landau, L.D. and Lifshitz, E.M., Fluid Mechanics, Addison-Wesley Publishing Co., Inc., Reading, Mass., 1959.

21. Vand, V., "Viscosity of Solutions and Suspensions,"
J. of Phys. and Colloid Chem., V.52, p. 277, (1948).
22. Jeffery, G.B., "The Motion of Ellipsoidal Particles
Immersed in a Viscous Fluid," Proc. Roy. Soc., V.A102,
p. 161, (1923).
23. Rubinow, S.I. and Keller, J.B., "The Transverse Force
on a Spinning Sphere Moving in a Viscous Liquid,"
Jour. Fluid Mech., V.11, p. 447, (1961).
24. Trevelyan, B., and Mason, S., "Particle Motions in
Sheared Suspensions. I. Rotations," J. of Colloid
Sci., V.6, No. 4, Aug. 1951.
25. Owen, P. and Zienkiewicz, H., "The Production of
Uniform Shear Flow in a Wind Tunnel," Jour. Fluid
Mech., V.2, p. 521, (1957).
26. Vidal, R.J., "The Influence of Two-dimensional Stream
Shear on Airfoil Maximum Lift," Jour. A/S Sci., V. 29,
No. 8, Aug. 1962.
27. Reichardt, H., "Über die Umströmung Zylindrischer
Körper in einer Geradlinigen Couetteströmung,"
Mitteilungen No. 9, Max-Planck-Institut für Stromungs-
forschung, Göttingen, 1954.

28. Reichardt, H., "Über die Geschwindigkeitsverteilung in einer geradlinigen turbulenten Couetteströmung," Z. angew. Math. Mech., Sonderheft 1956, p. 826.
29. Handbook of Chemistry and Physics, 38th Edition, Chemical Rubber Publishing Co., Cleveland, Ohio, 1956.
30. Bretherton, F.P., "Slow Viscous Motion Round a Cylinder in a Simple Shear," Jour. Fluid Mech., V.12, No. 4, April 1962.
31. Thom, A., "An Investigation of Fluid Flow in Two Dimensions," Aero. Res. Coun. Rep., Memo 1194, 1927.
32. Kawaguti, M., "Numerical Solution of the Navier-Stokes Equations for the Flow around a Circular Cylinder at Reynolds Number 40," J. Phys. Soc. Japan, V.8, No. 6, p. 747, 1953.
33. White, C.M., "The Drag of Cylinders in Fluids at Slow Speeds," Proc. Royal Society, V. A186, p. 472, (1946).
34. Bairstow, L., Cave, B., and Lang, E., "The Two-dimensional Slow Motion of Viscous Fluids," Proc. Royal Society, Ser. A, p. 394, (1922).

35. Wisselsberger, C., "Neuere Feststellungen uber die Gesetze des Flussigkeits-und Luftwiderstandes," Phys. Zeit., V.22, p. 321, (1921).
36. Relf, E.F., "Discussion of the Results of Measurements of the Resistance of Wires, with some Additional Tests on the Resistance of Wires of Small Diameter," ARC Report 102, 1914.
37. Tritton, D.J., "Experiments on the Flow Past a Circular Cylinder at Low Reynolds Numbers," Jour. Fluid Mech., V.6, No. 4, Nov. 1959.
38. (a) Brenner, H., "Effect of Finite Boundaries on the Stokes Resistance of an Arbitrary Particle," Jour. Fluid Mech., V.12, No. 1, Jan. 1962.
38. (b) Brenner, H., "The Oseen Resistance of a Particle of Arbitrary Shape," Jour. Fluid Mech., V.11, No. 4, Dec. 1961.
39. Hoerner, S.F., Fluid-Dynamic Drag, Published by the Author, Midland Park, New Jersey, 1958.
40. Taylor, G.I., "Stability of a Viscous Liquid Contained Between Two Rotating Cylinders," Phil. Trans. A, Vol. 223, p. 289, (1923).

41. Reichardt, H., "Gesetzmässigkeiten der geradlinigen turbulenten Couetteströmung," Max-Planck-Inst. für Strömungsforschung, Göttingen, Mitt. 22, 1959.
42. Wasow, W., "One Small Disturbance of Plane Couette Flow," J. Res. Nat. Bur. Stand., V.51, p. 195, 1953.
43. Hopf, L., "Verlauf kleiner Schwingungen auf einer Strömung reibender Flüssigkeit," Ann. d. Physik, Bd. 44, 1914.
44. Von Mises, R., "Kleine Schwingungen und Turbulenz," Jahresbericht der deutschen Mathematiker-Vereinigung, V. 21, p. 241, 1912.
45. Von Mises, R., "Beitrag zum Oszillationsproblem," Festschrift Heinrich Weber, p. 262; Leipzig und Berlin, 1912.
46. Lin, C.C., The Theory of Hydrodynamic Stability, Cambridge Univ. Press, 1955.
47. Orr, M., "The Stability or Instability of the Steady Motions of a Liquid," Proc. Roy. Irish Academy, A., V.27, p. 128, 1907.
48. Shen, S.F., "Calculated Amplified Oscillations in Plane Poiseuille and Blasius Flows," J. Aero. Sci., V.21, p. 62, 1954.

49. Lessen, M., "On Stability of Free Laminar Boundary Layer Between Parallel Streams," NACA TR 979, 1950.
50. Scott, R., and Young, R., "Drag of a Free Falling Sphere," MIT 16.62 Lab Report, May 1962.
51. Thomas, T.N., "Examination of Instabilities of a Rectilinear Shear Flow," MIT 16.62 Lab Report, Dec., 1962.

TABLE 1

TANK PROPERTIESTank 1

Length	29,3"
Width	13,3"
Depth	11.5"
Test section length	22,5"
Test section width	4,85"
Belt width	7.5"
Power Source	1/2 hp AC electric motor
Speed control	"Vickers" hydraulic transmission (Model AA16801A)

Tank 2

Length	45"
Width	17"
Depth	7"
Test Section length	36"
Test Section width	6"
Belt width	5"
Power source	1/3 hp AC electric motor
Speed control	"Zeromax" mechanical transmission (Model M143)

TABLE 2
PARAMETER RANGE IN CYLINDER EXPERIMENTS

	<u>Minimum</u>	<u>Maximum</u>	<u>Ratio</u>
cylinder diameter	.0122 inches	.500 in.	41
cylinder length/cylinder diameter	7.48	280	37.4
test section width/cyl. diameter	9.63	492	51.1
relative velocity at cylinder	.00262 ft/sec	.130 ft/sec	49.7
fluid kinematic viscosity	93 centistokes	637 cs.	6.85
shear rate	.0595 sec ⁻¹	1.94 sec ⁻¹	32.6
Reynolds number	6.6 x 10 ⁻⁴	1.8	2730

TABLE 3

PARAMETER RANGE IN SPHERE EXPERIMENTS

<u>Parameter</u>	<u>Minimum</u>	<u>Maximum</u>	<u>Ratio</u>
sphere diameter, d_s	.25 in.	.50 in.	2
cylinder diameter, d_c	.0122 in.	.0647 in.	5.3
d_s/d_c	7.73	20.5	2.65
L_c/d_s	3.92	6.16	1.57
H/d_s	9.65	19.3	2.0
relative velocity at sphere	.00535 ft/sec	.074 ft/sec	13.8
fluid kinematic viscosity	104 cs.	545 cs.	5.24
shear rate	.0641 1/sec	1.1 sec ⁻¹	17.2
Reynolds number	3.8×10^{-2}	2.3	26.3

TABLE 4

AMPLITUDE OF PRIMARY DISTURBANCES IN COUETTE FLOW

<u>Re_s</u>	<u>Amplitude</u>
13,500	.43 H
17,000	.43 H
20,800	.42 H
32,000	.43 H

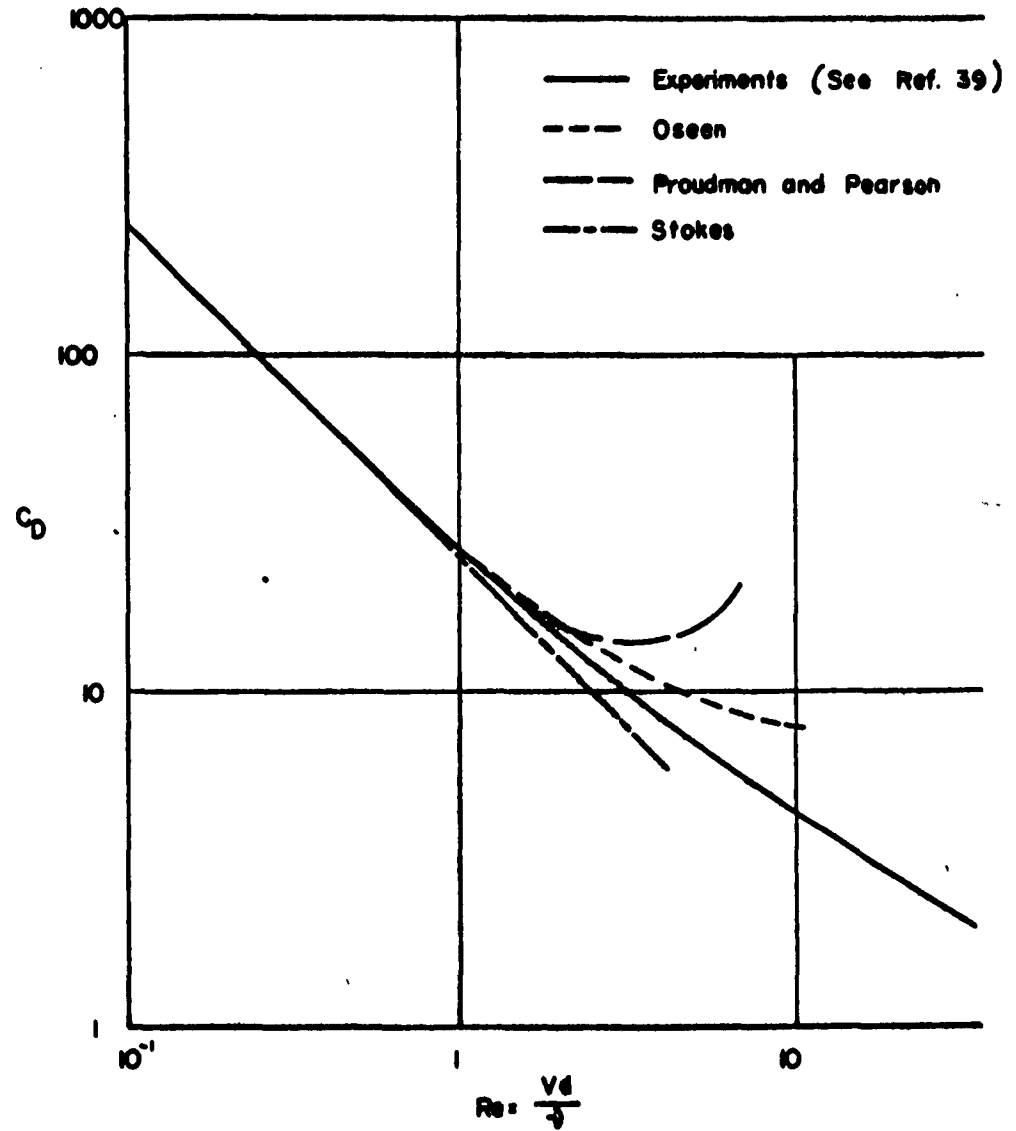


FIG. 1 - Drag Coefficient of a Sphere in Uniform Flow

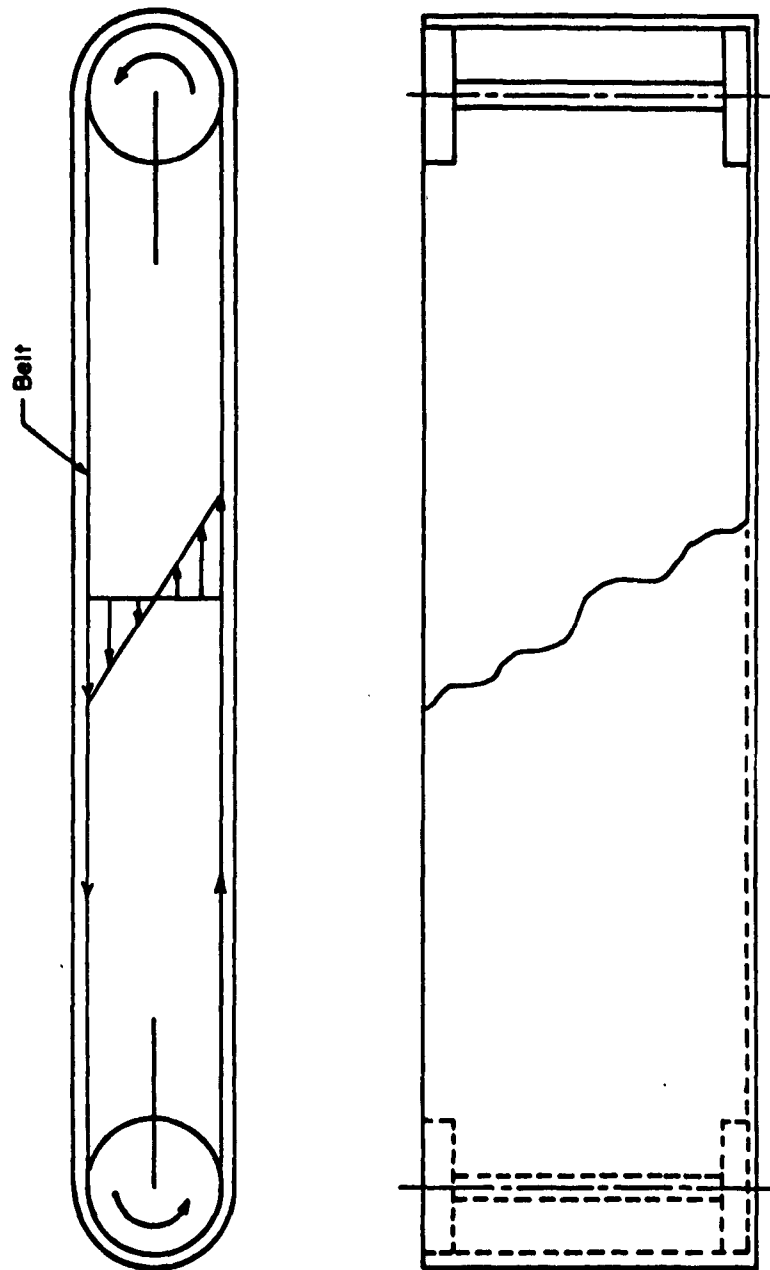
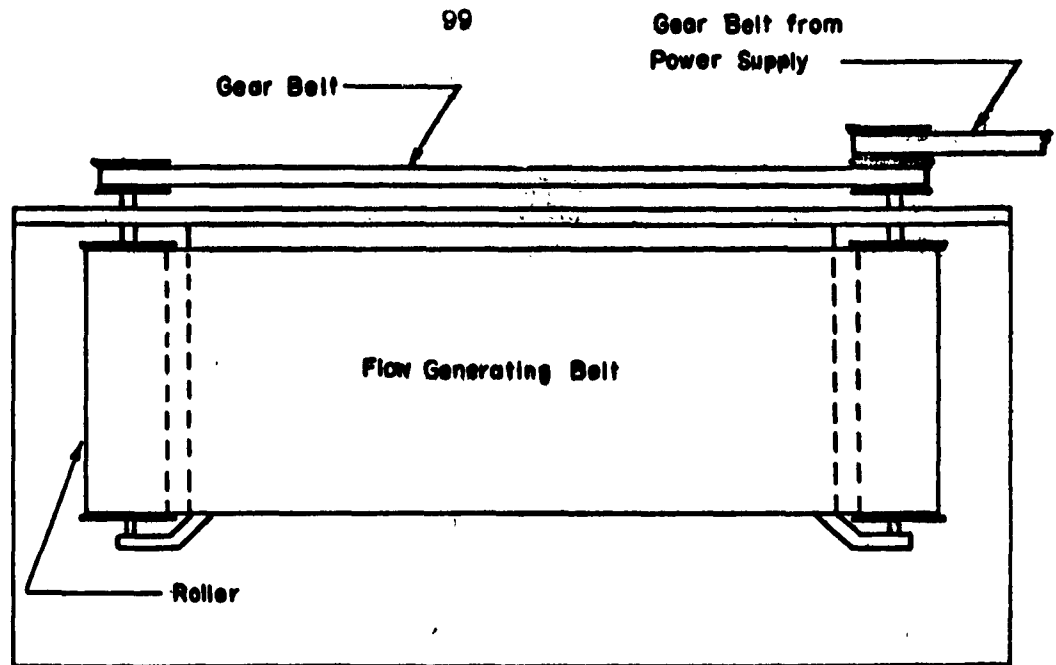
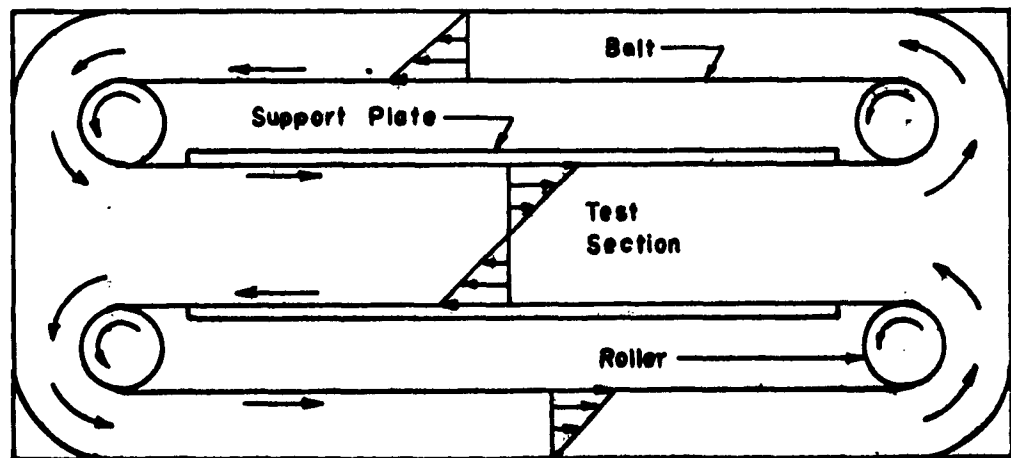


Fig. 2 - Schematic Drawing of Reichardt's Shear Flow Tank



Side View



Top View

Fig. 3 - General Arrangement of Shear Flow Tank Components

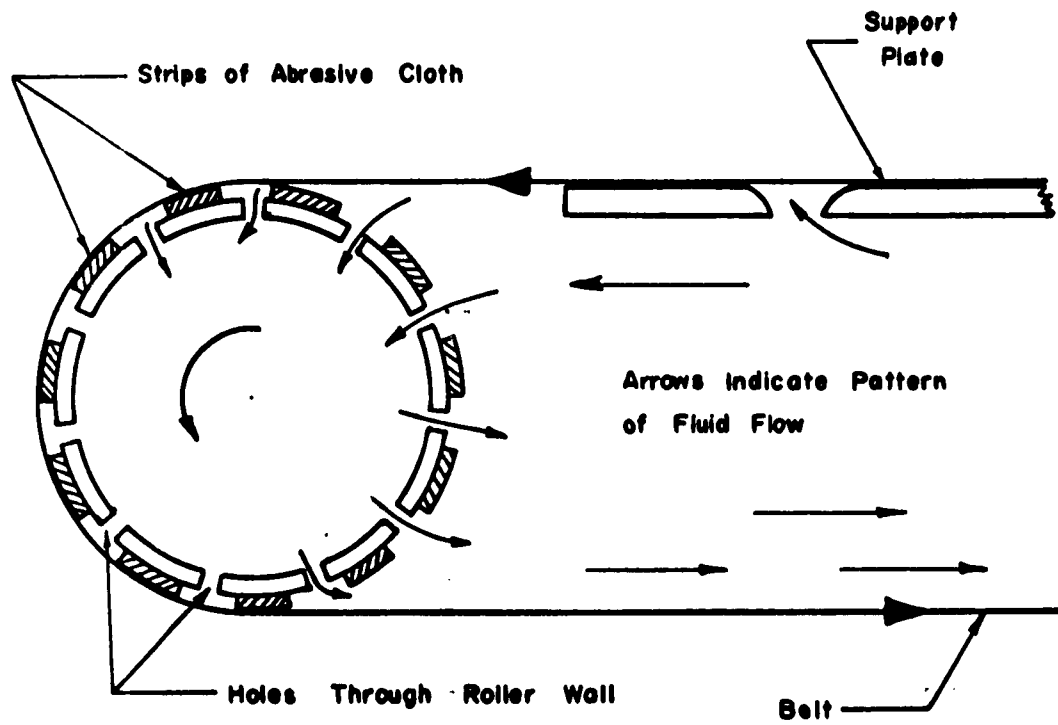


Fig. 4 - Details of Belt, Roller, and Supporting Plate Arrangement

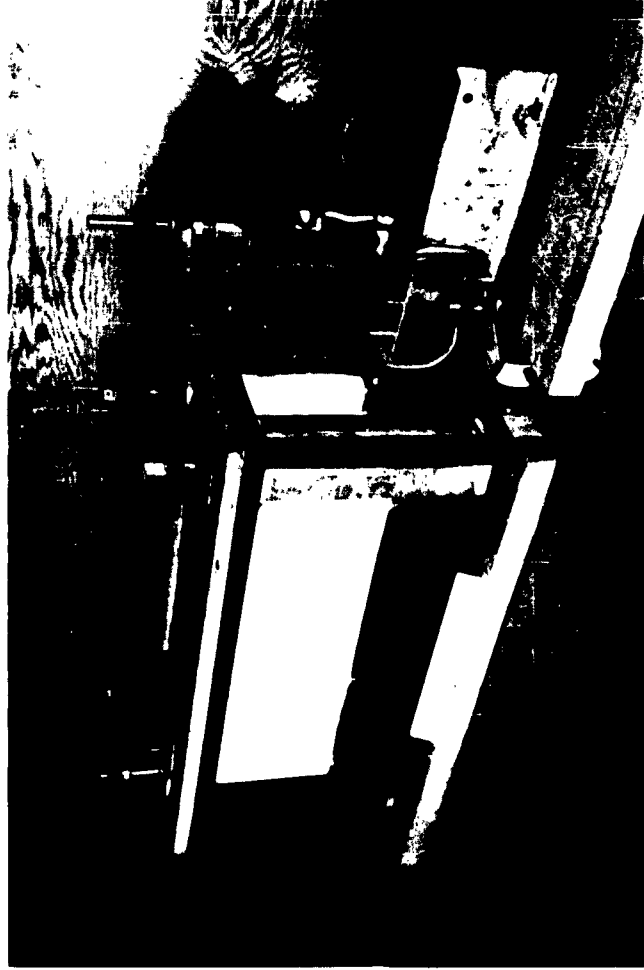


Fig. 5 - Photograph of Tank 1



Fig. 6 - Photograph of Tank 2

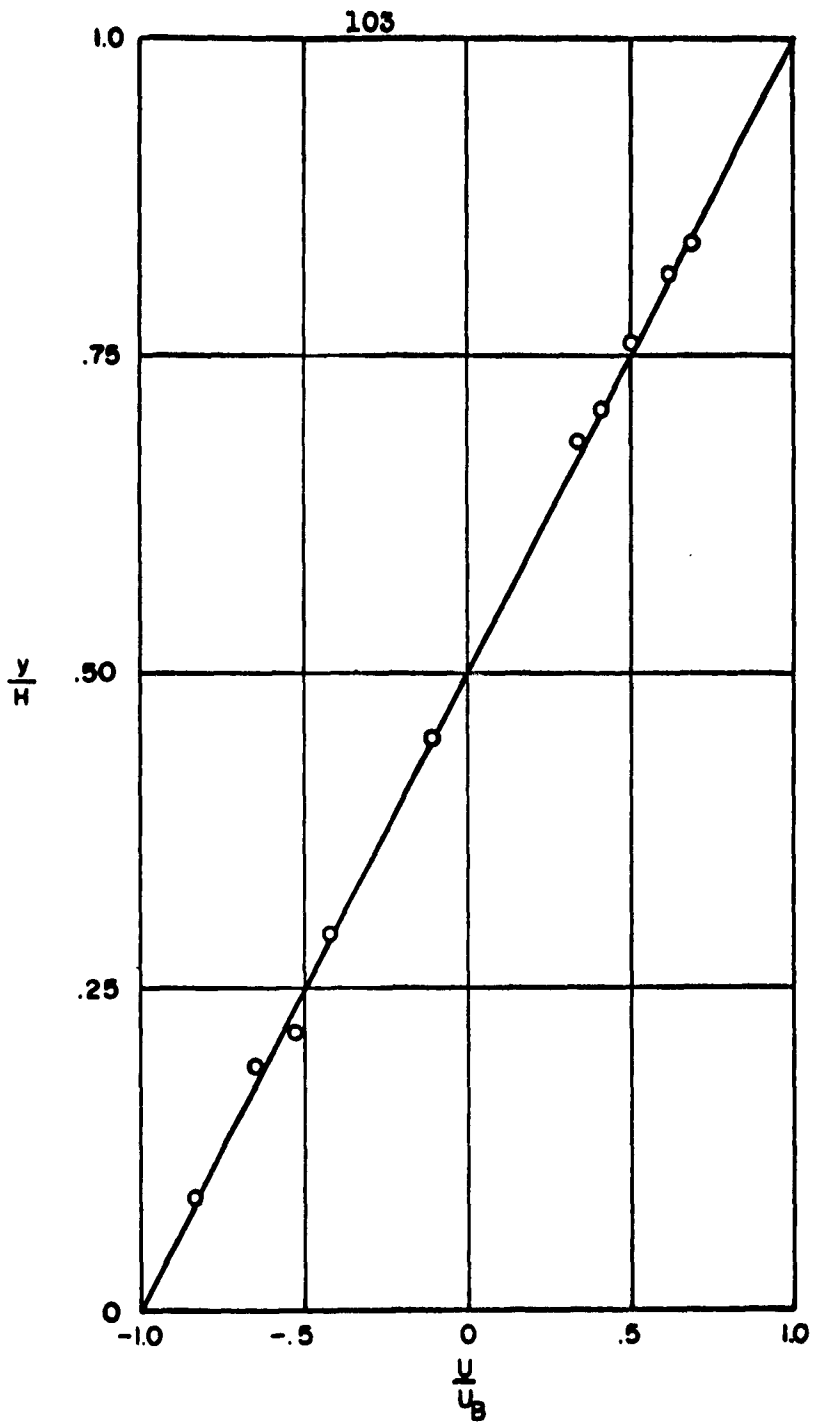


Fig. 7 - Velocity Profile in Test Section at Surface, $Re_B = 28$

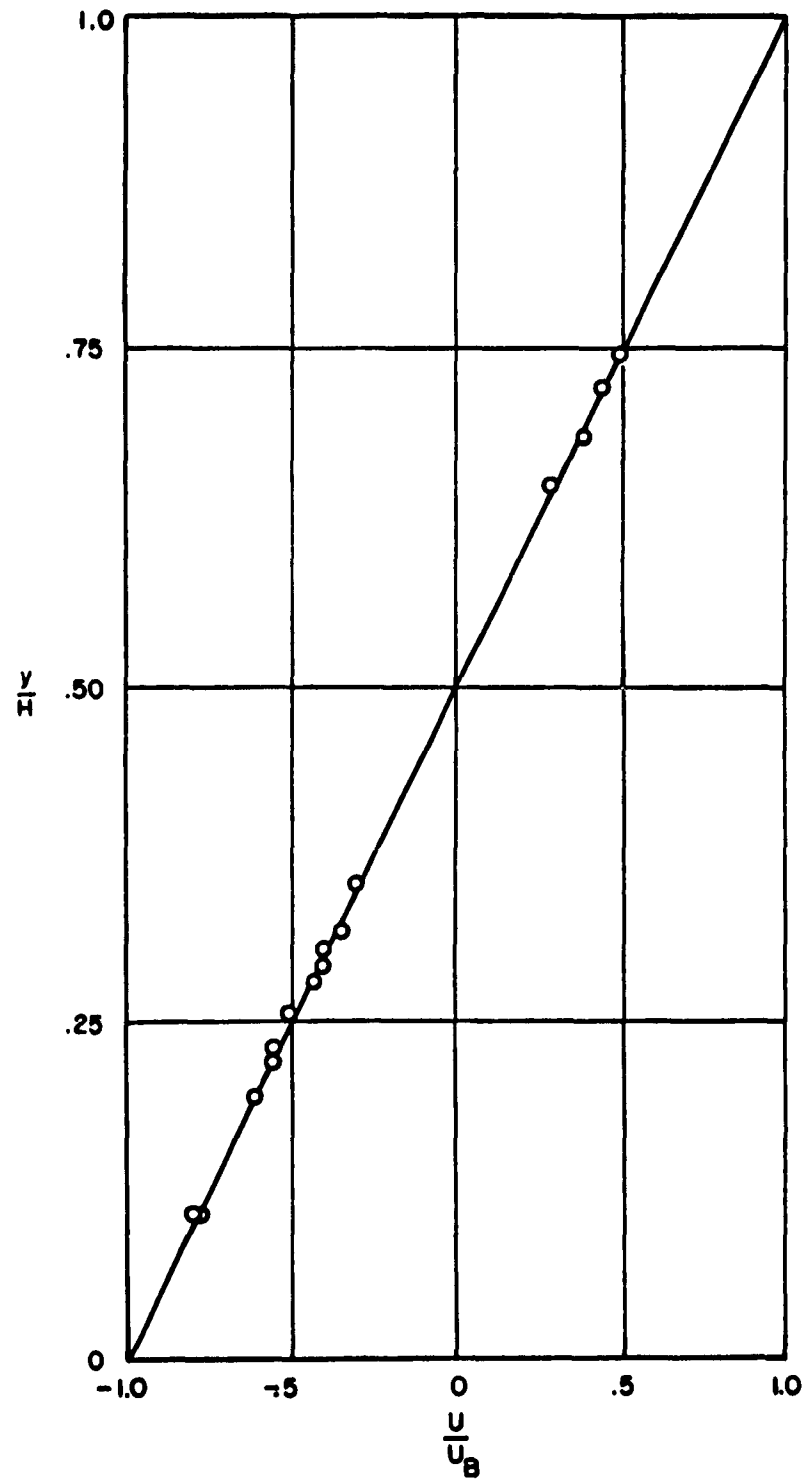


Fig. 8 - Velocity Profile in Test Section at Surface, $Re_s = 48$

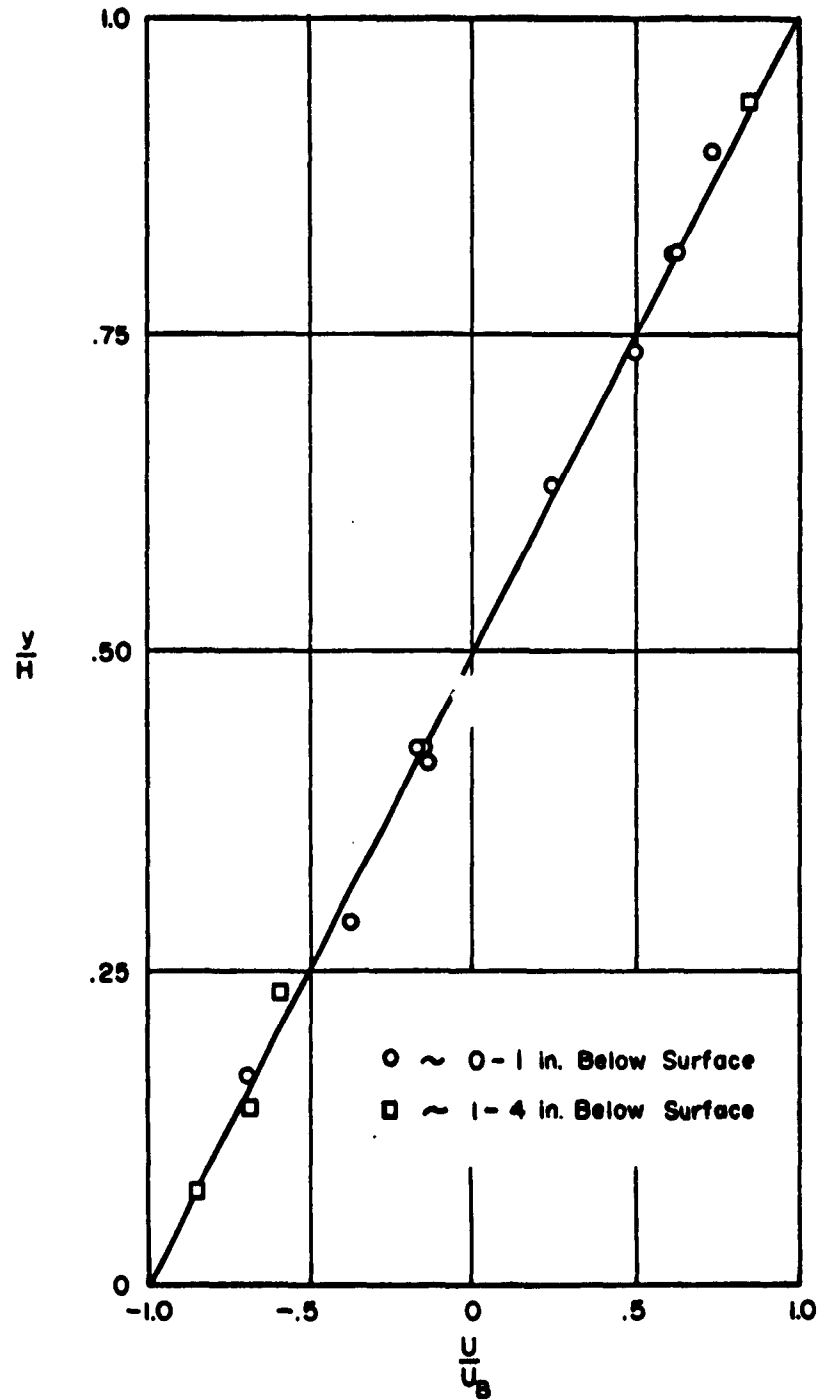


Fig. 9 - Velocity Profile in
Test Section, $Re_s=55$

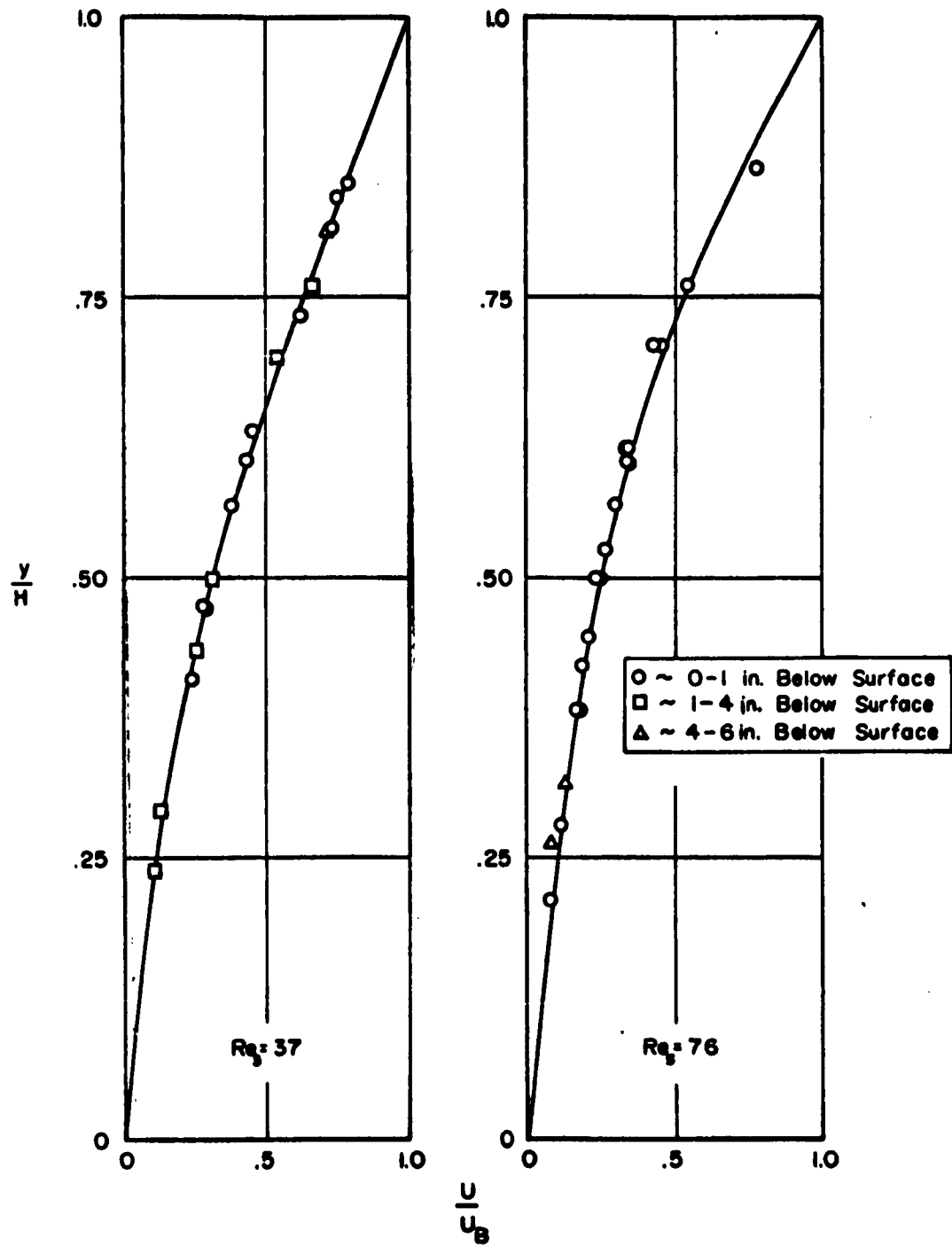


Fig. 10 - Velocity Profile With One Belt Stationary, $\frac{\Delta}{H} = 4.65$



$Re_s = 104$



$Re_s = 83$

Fig. 11 - Streak Photographs of Shear Flow With One Belt Stationary, $\frac{A}{H} = 13$

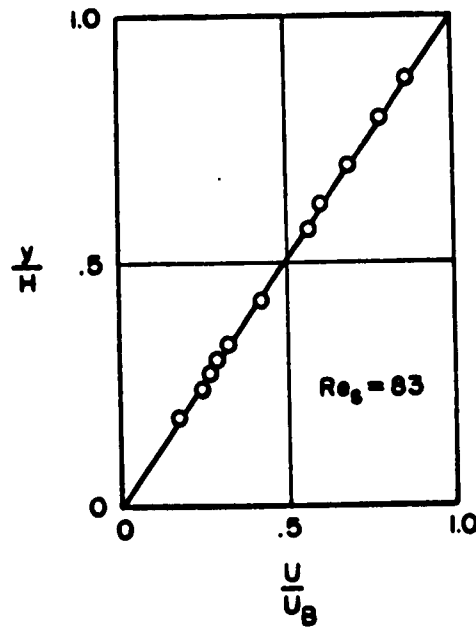
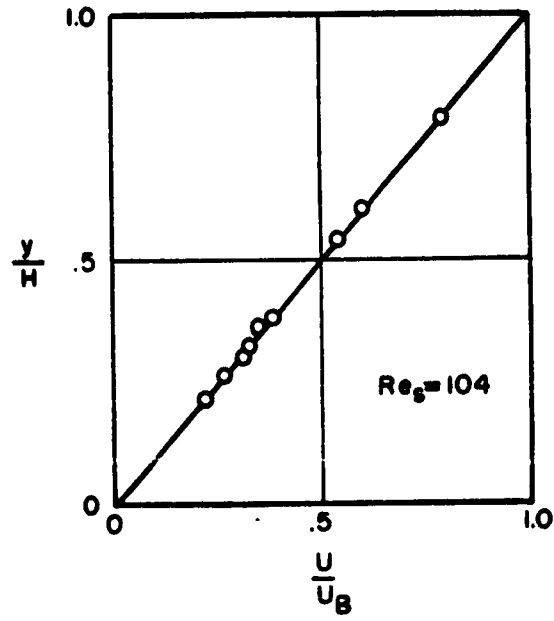
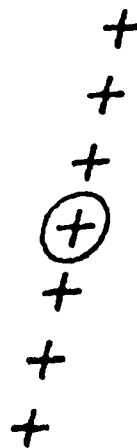


Fig. 12 - Velocity Profiles With One Belt Stationary, $\frac{U}{H} = 13$

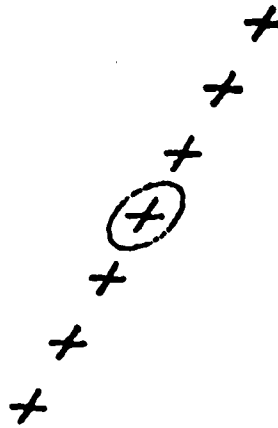


(a)

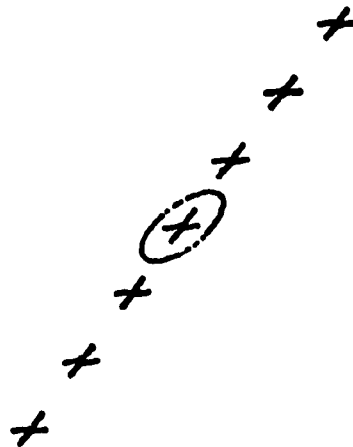


(b)

Fig. 13 - Deformation of a Surface Pattern in
Rectilinear Couette Flow
(Photos taken at 5 second intervals)

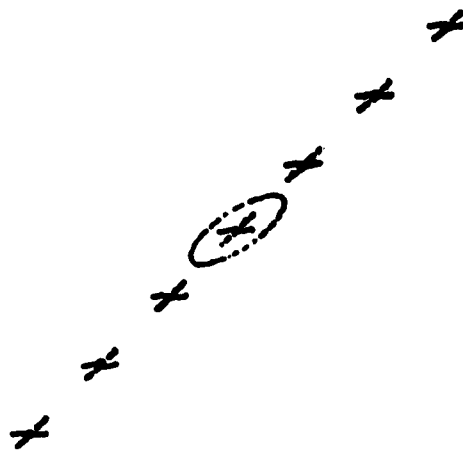


(c)



(d)

Fig. 13 - Continued



(e)



(f)

Fig. 13 - Continued

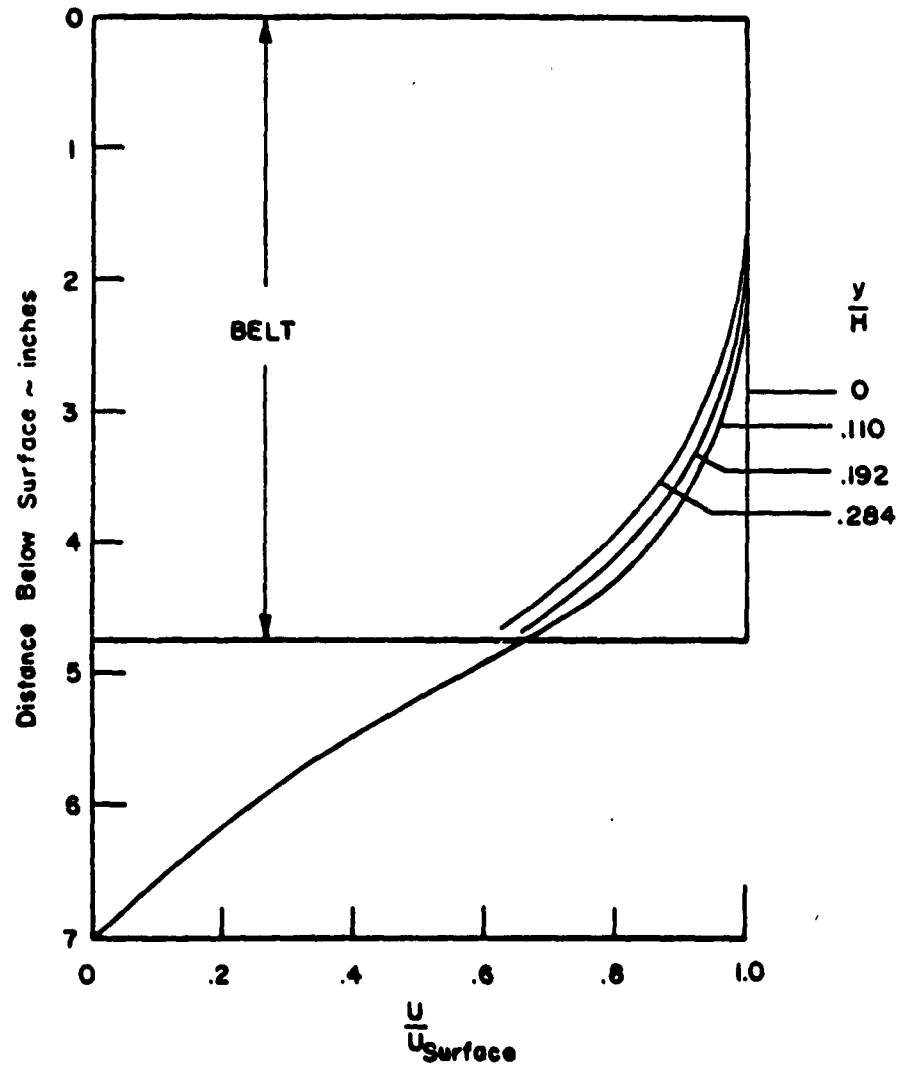
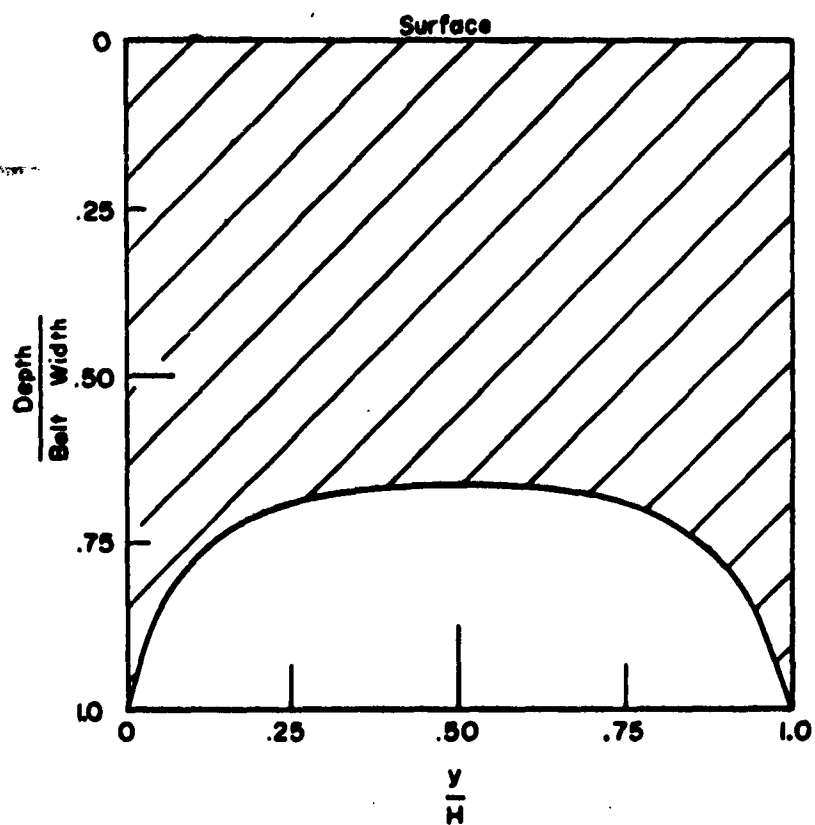


Fig. 14 - Velocity Profiles in Planes Parallel to the Belts, Tank 2



The Velocity in the Shaded Area is within
10% of the Velocity at the Surface for
Constant $\frac{y}{H}$

Fig. 15 - Approximate Depth of
Two-dimensional Flow,
Tank 2



Fig. 16 - Typical Vertical Velocity Profile Photograph

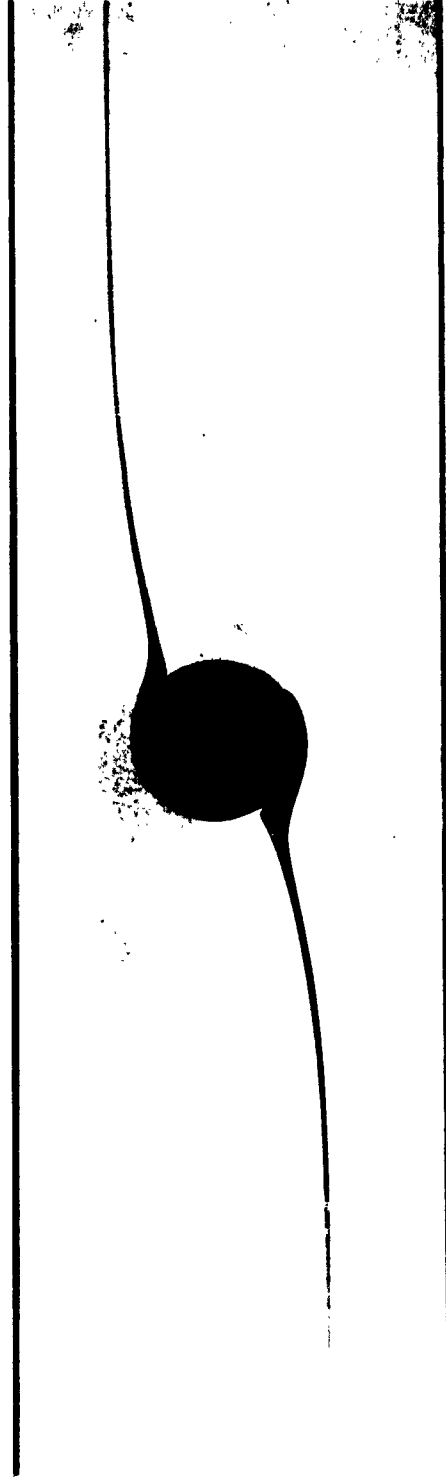


Fig. 17 - Symmetric Shear Flow Past a Circular Cylinder

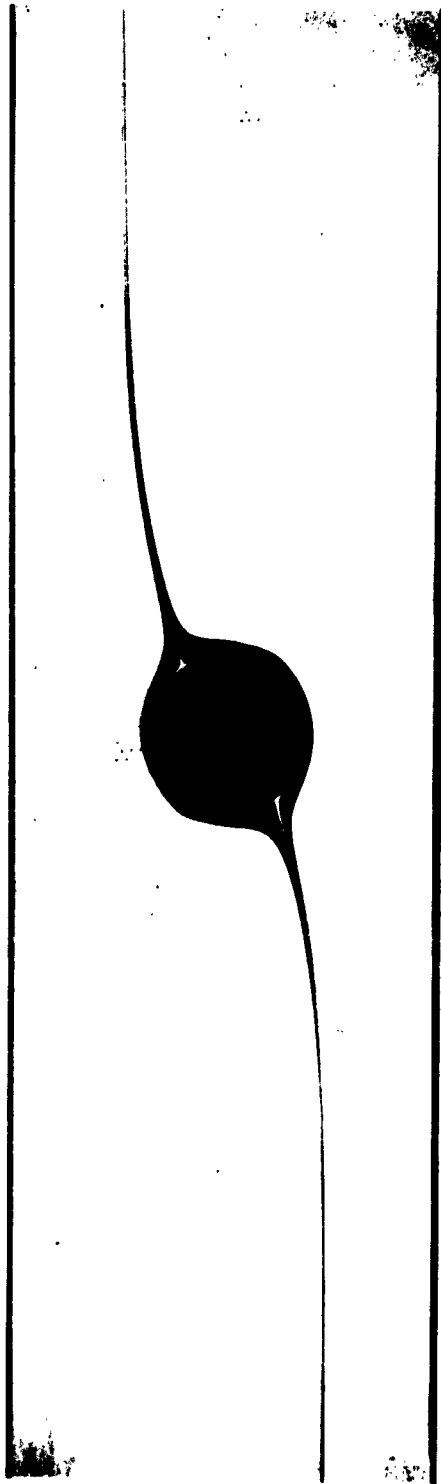


Fig. 18- Symmetric Shear Flow Past a Circular Cylinder

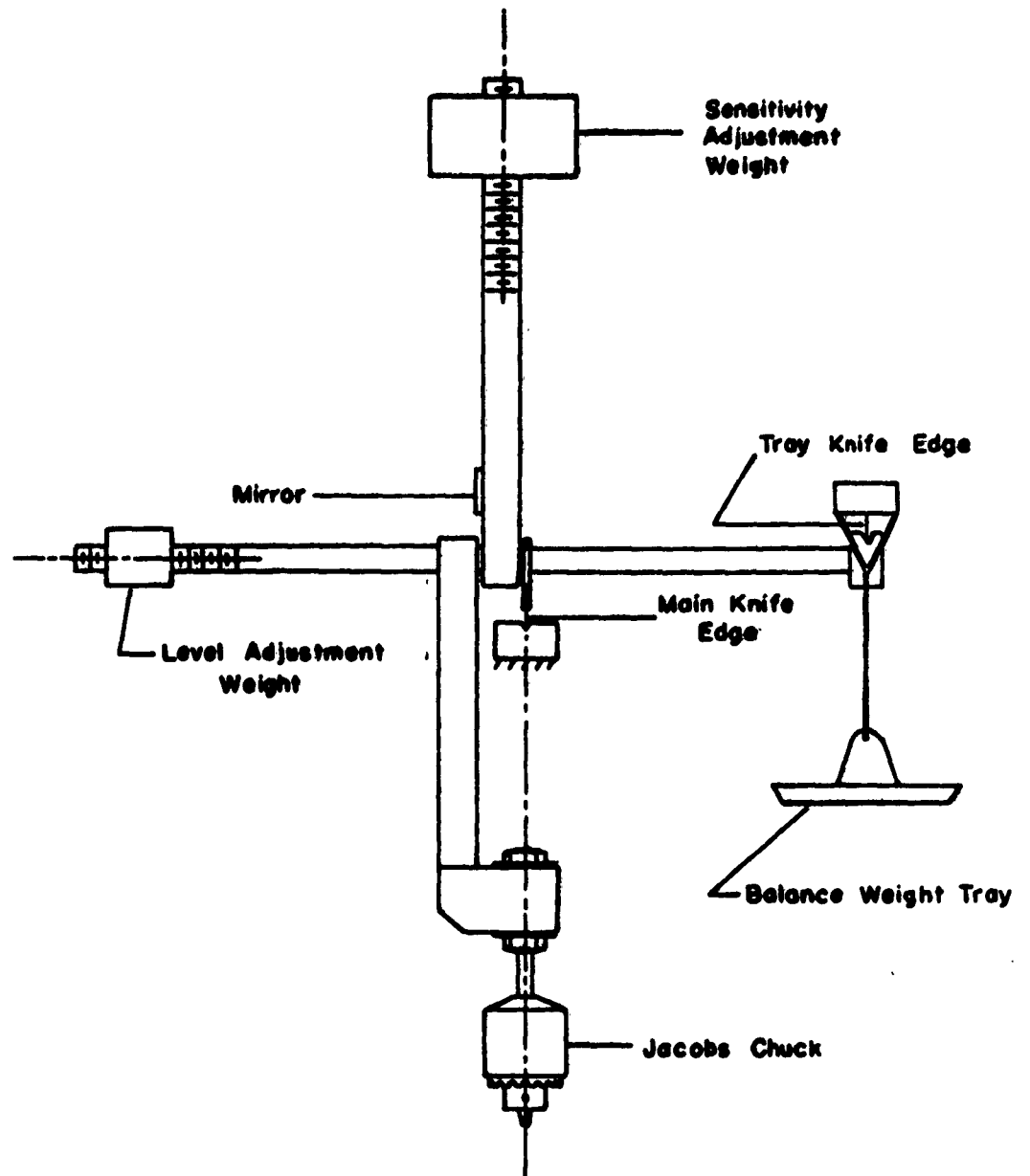


Fig. 19 - Schematic Drawing of Beam Balance

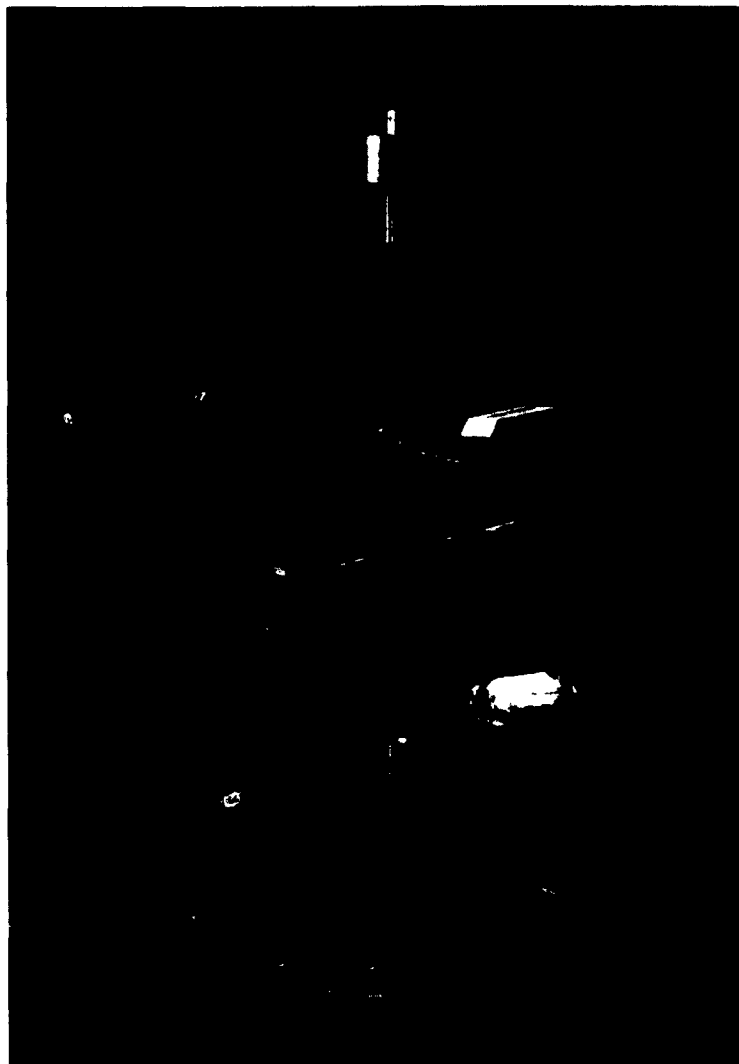


Fig. 20 - Photograph of Balance System



Fig. 21 - Test Setup, Tank 2

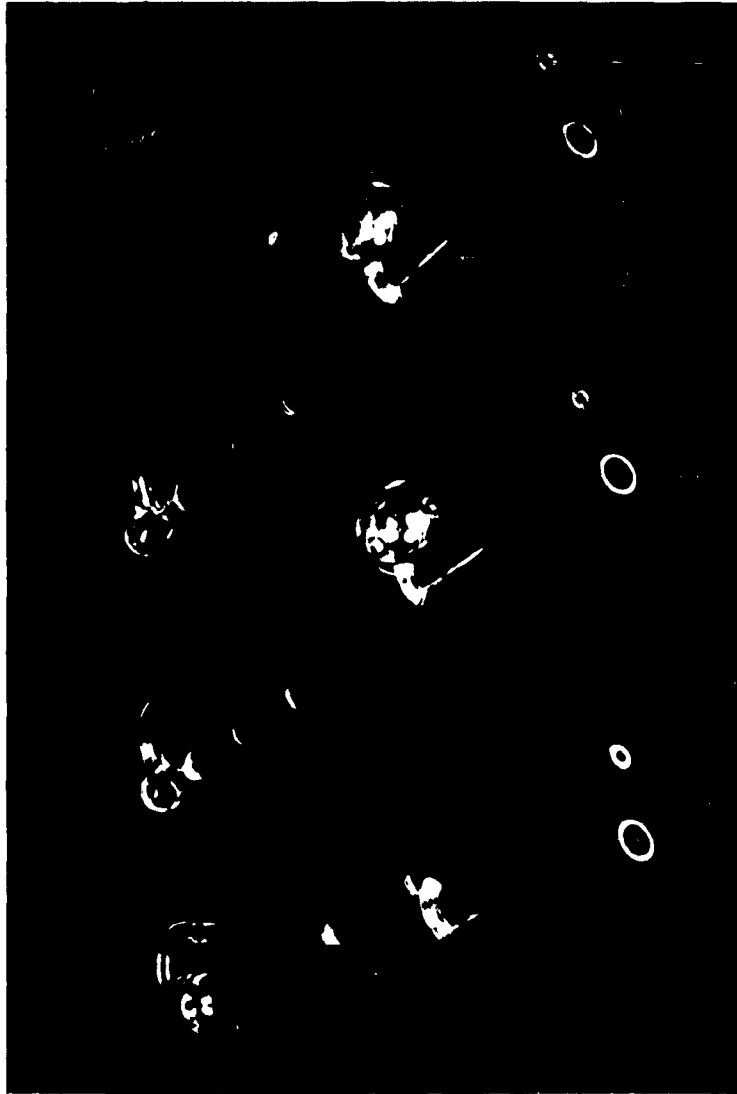


Fig. 22 - Cannon-Fenske Viscometers

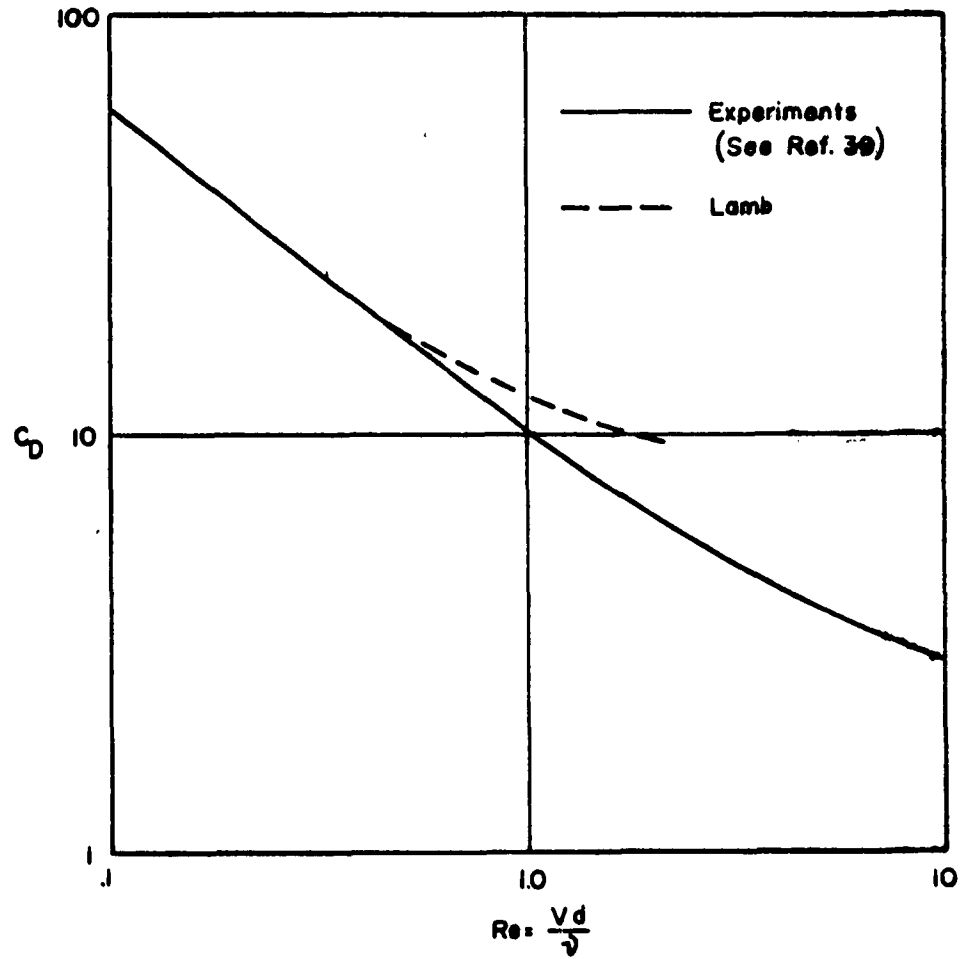


Fig. 23 - Drag Coefficient of a Circular Cylinder in Uniform Flow



Fig. 24 - Cylinders Used in Drag Experiments

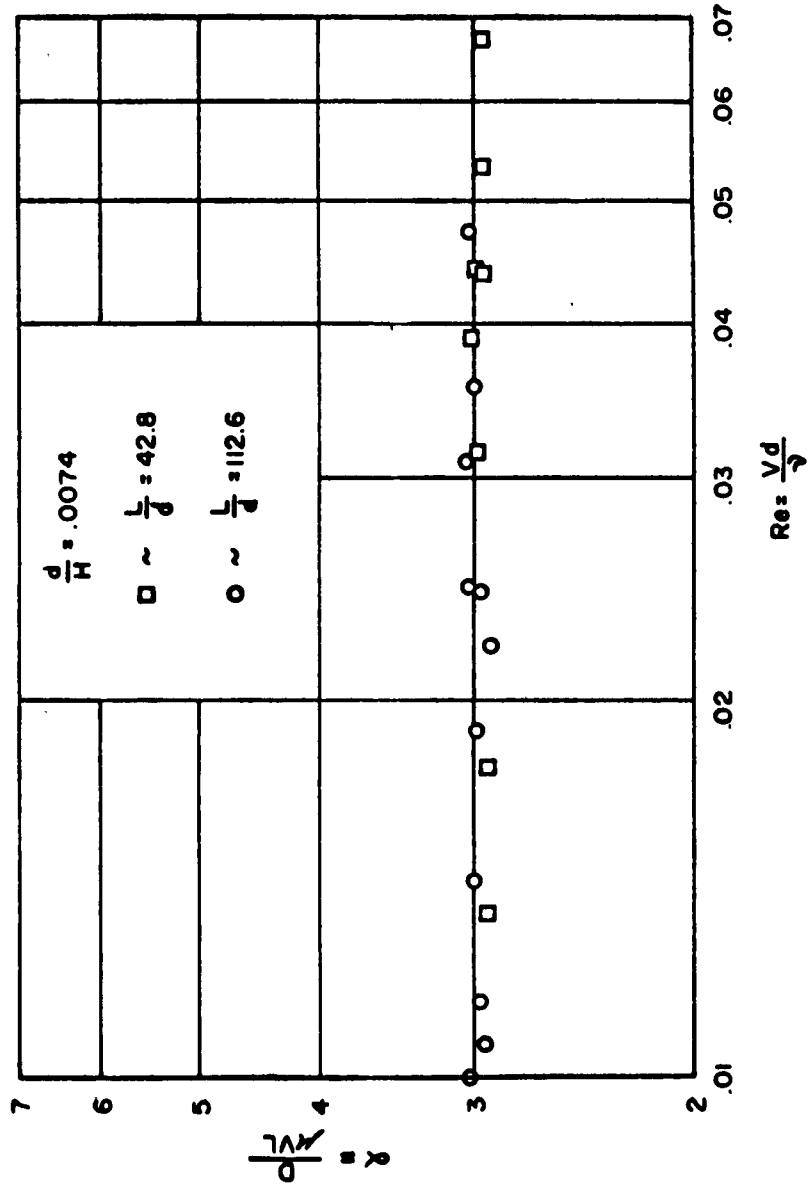


FIG. 25 - Effect of Aspect Ratio on Drag of a Circular Cylinder
 $\frac{d}{H} = .0074, \frac{L}{H} = \frac{1}{3}$

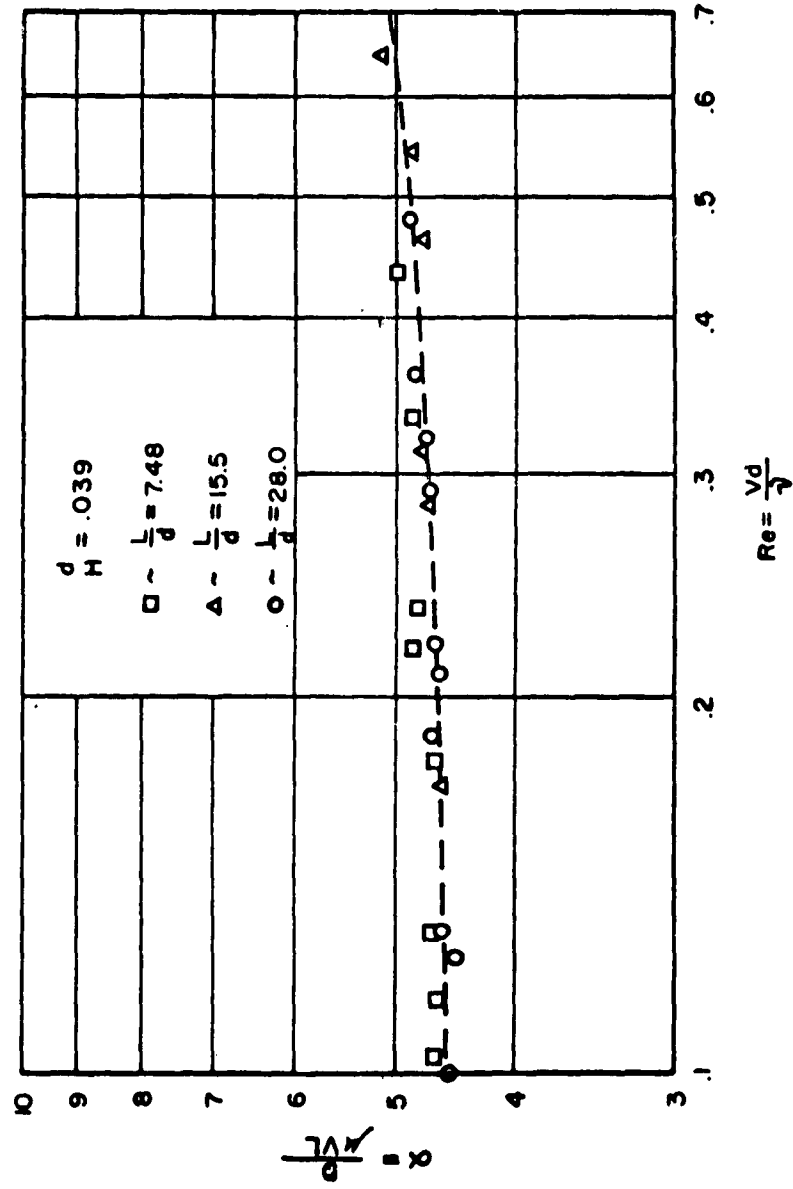


Fig. 26 - Effect of Aspect Ratio on Drag of a Circular Cylinder,
 $\frac{d}{H} = .039, \nu/H = \frac{1}{3}$

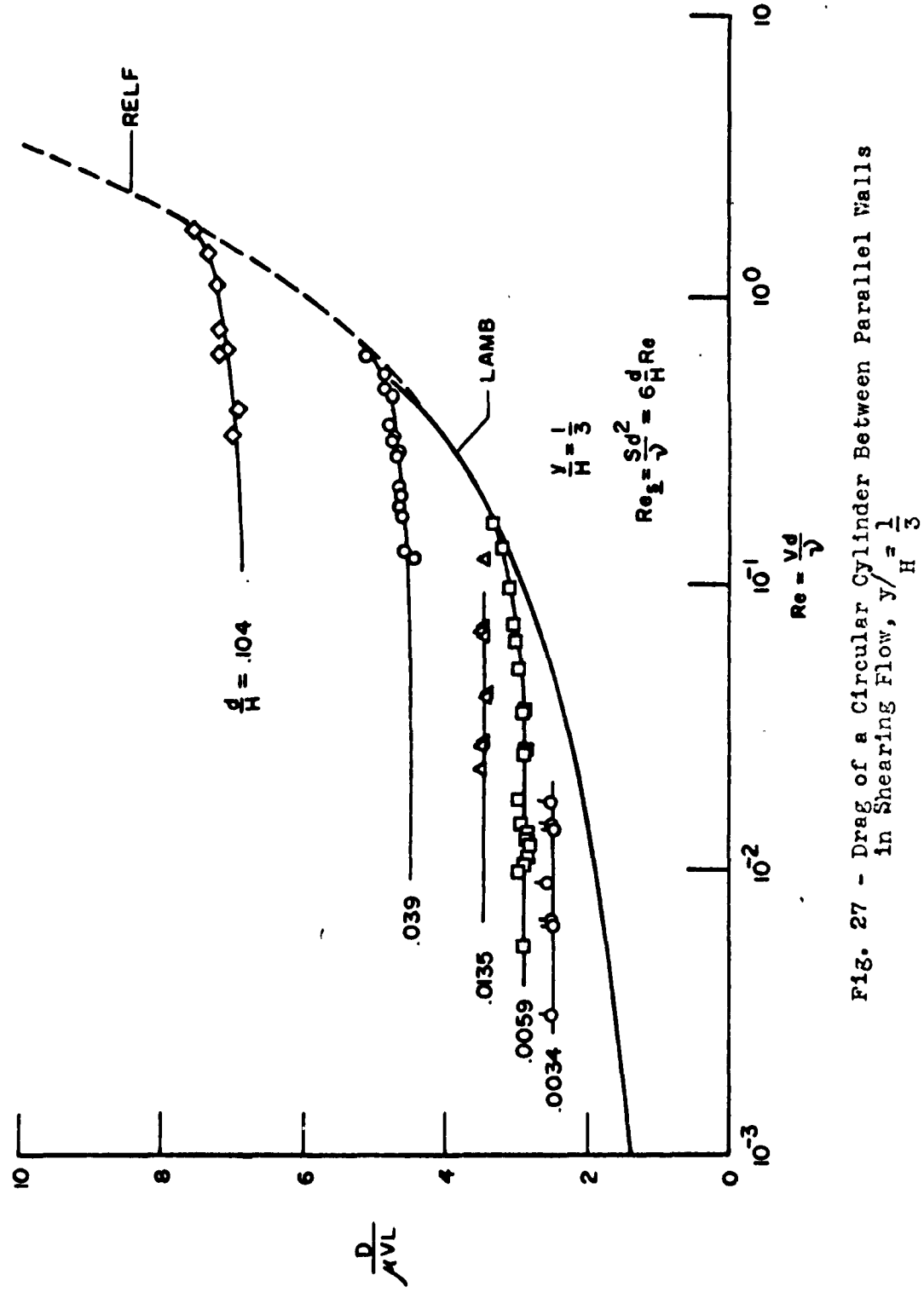


FIG. 27 - Drag of a Circular Cylinder Between Parallel Walls
 in Shearing Flow, $\frac{y}{H} = \frac{1}{3}$

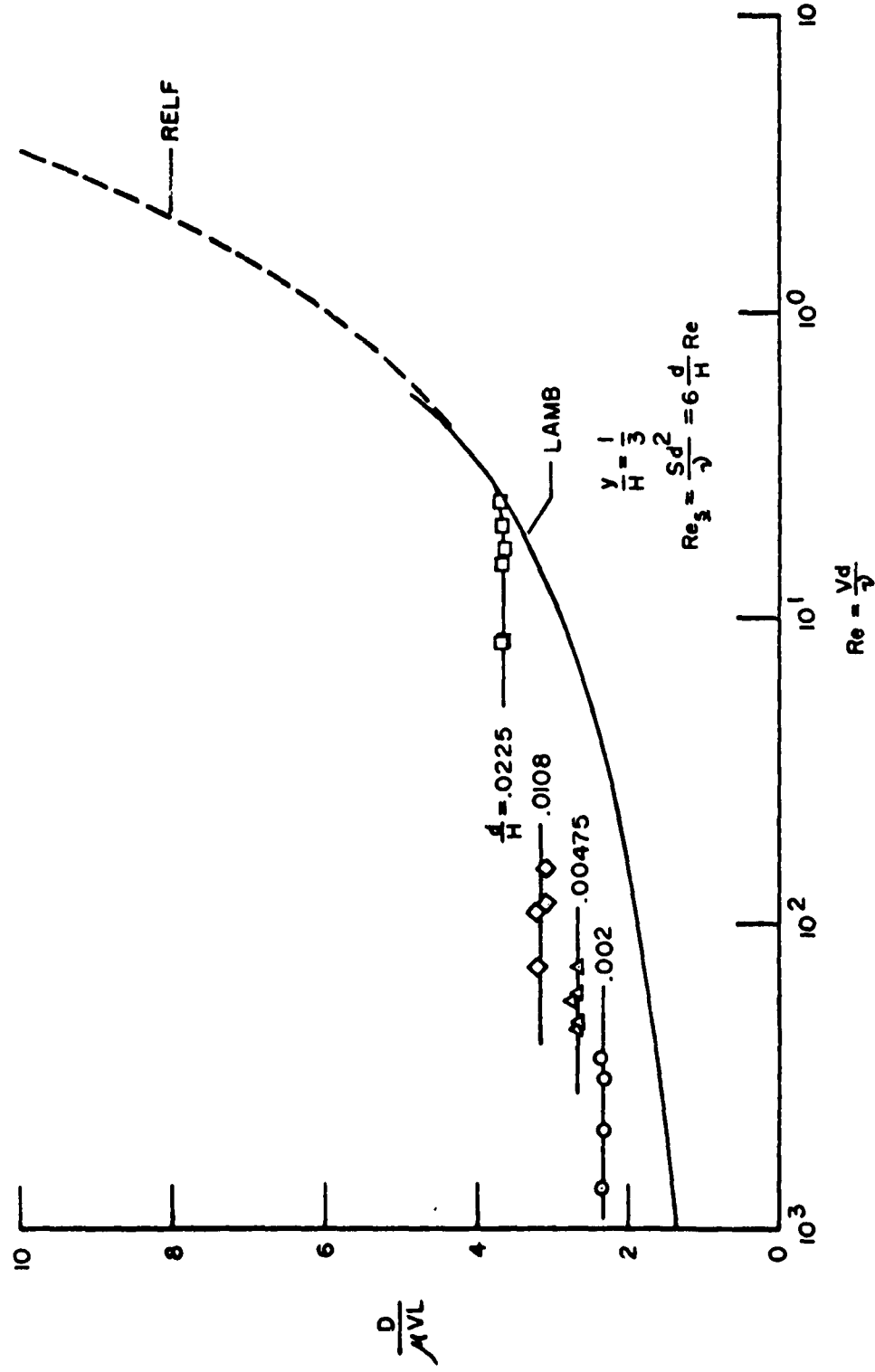


Fig. 28 - Drag of a Circular Cylinder Between Parallel Walls in Shearing Flow, $y/H = \frac{1}{3}$

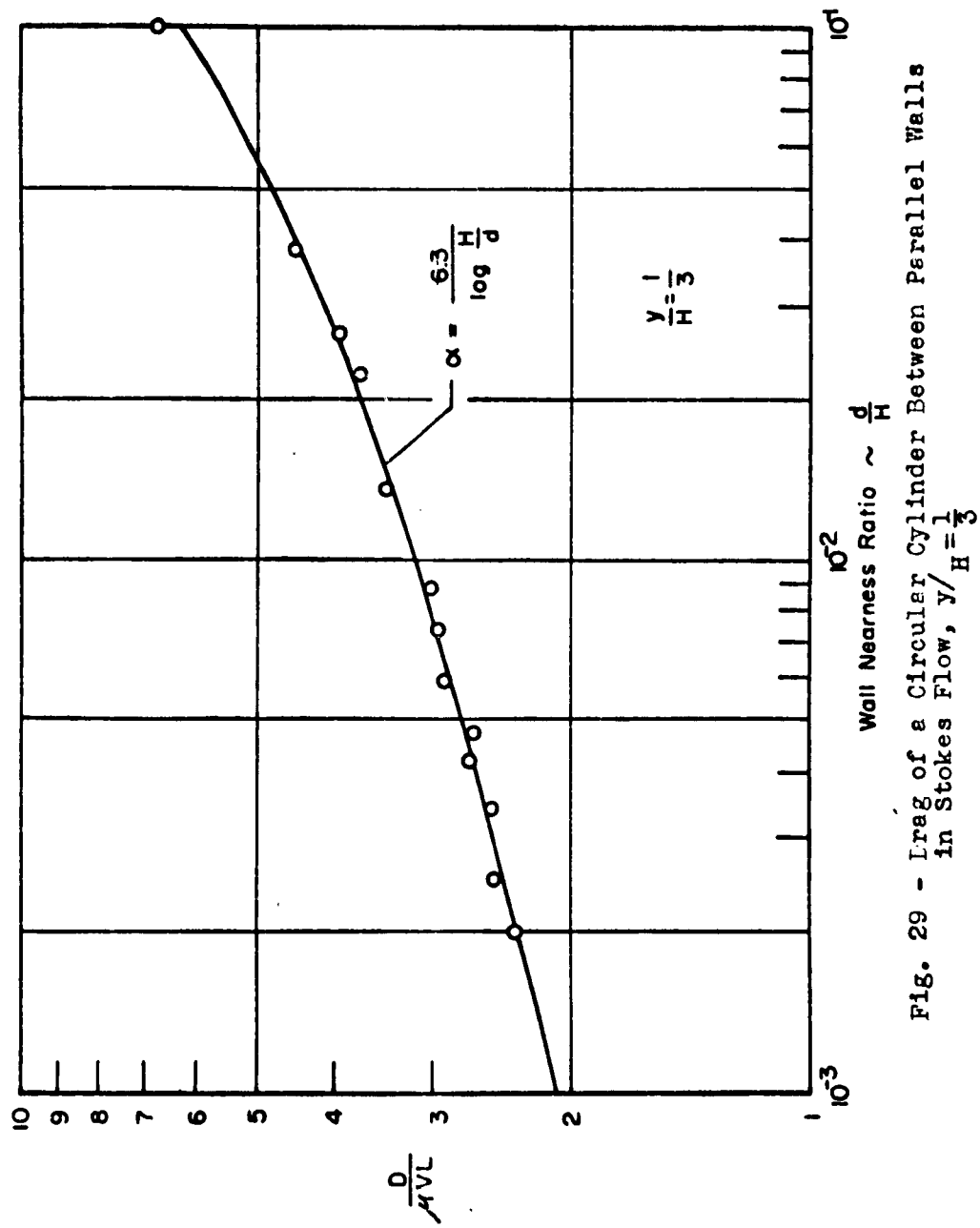


Fig. 29 - Drag of a Circular Cylinder Between Parallel Walls in Stokes Flow, $y/H = \frac{1}{3}$

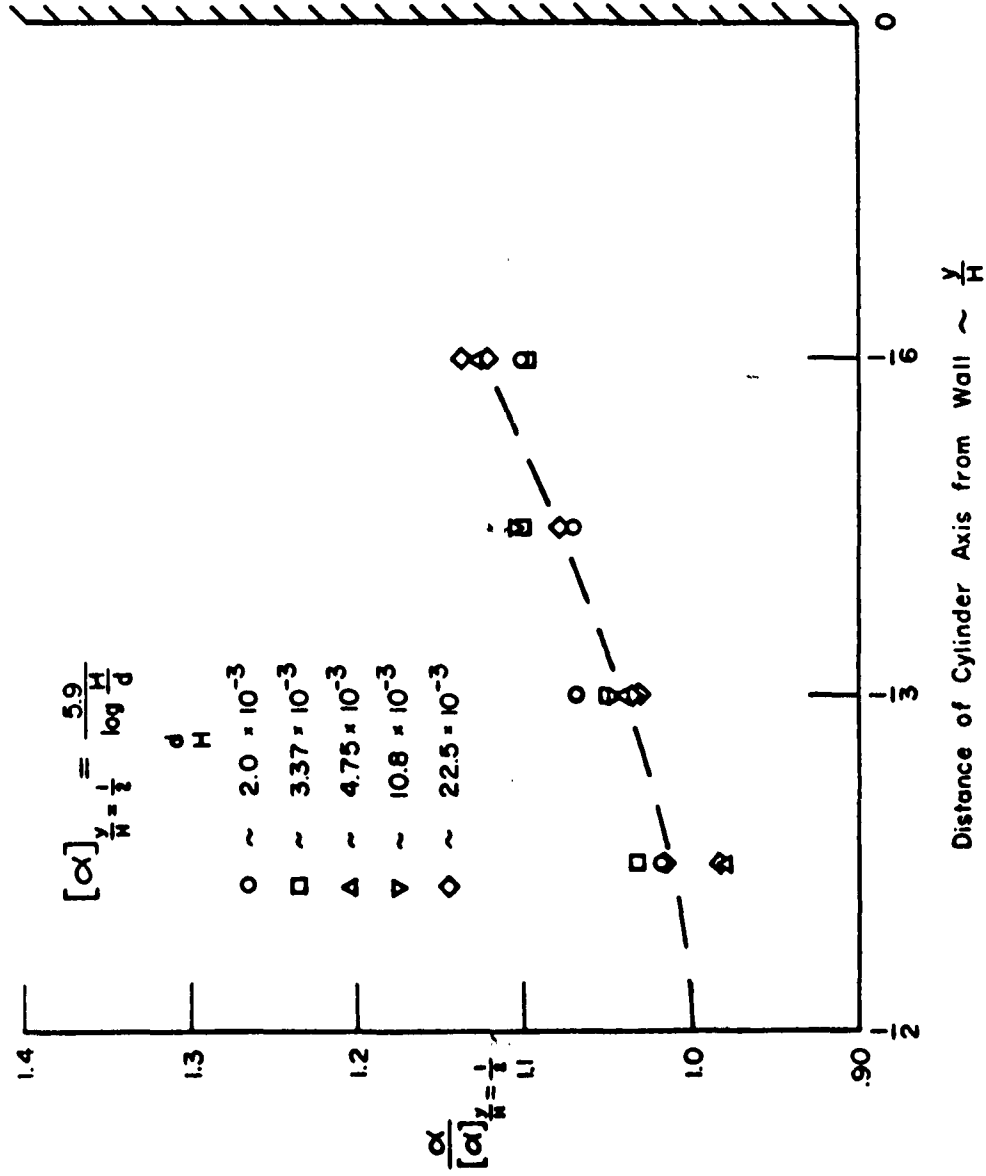


Fig. 30 - Effect of Lateral Position on Drag of a Circular Cylinder Between Parallel Walls in Stokes Flow

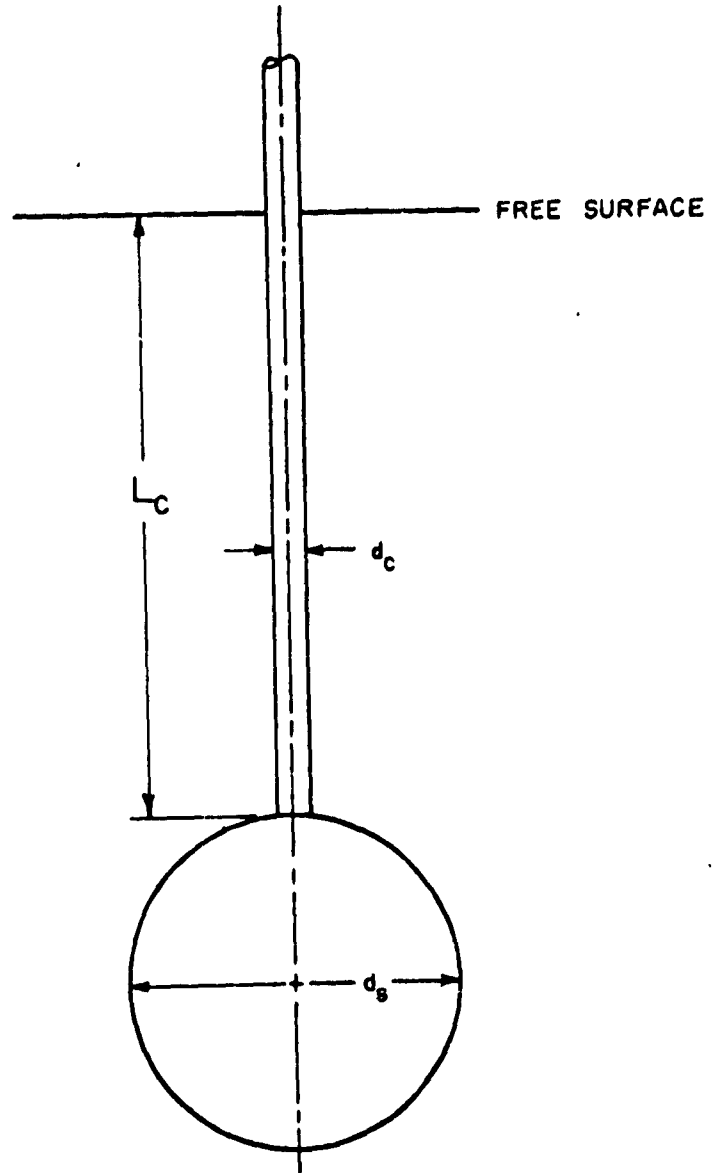


Fig. 31 - Geometry of Sphere and
Cylinder Mounting

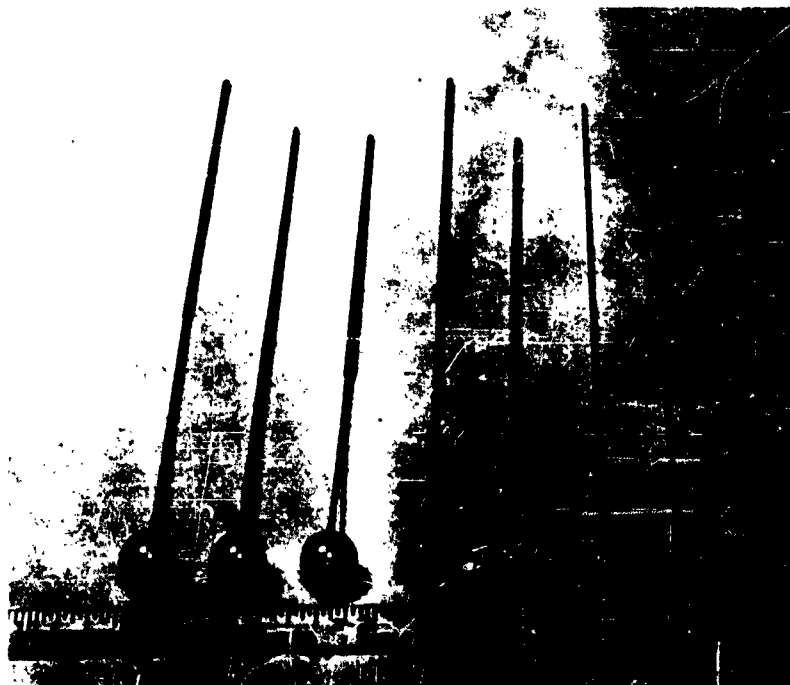


Fig. 32 - Spheres used in Drag Tests

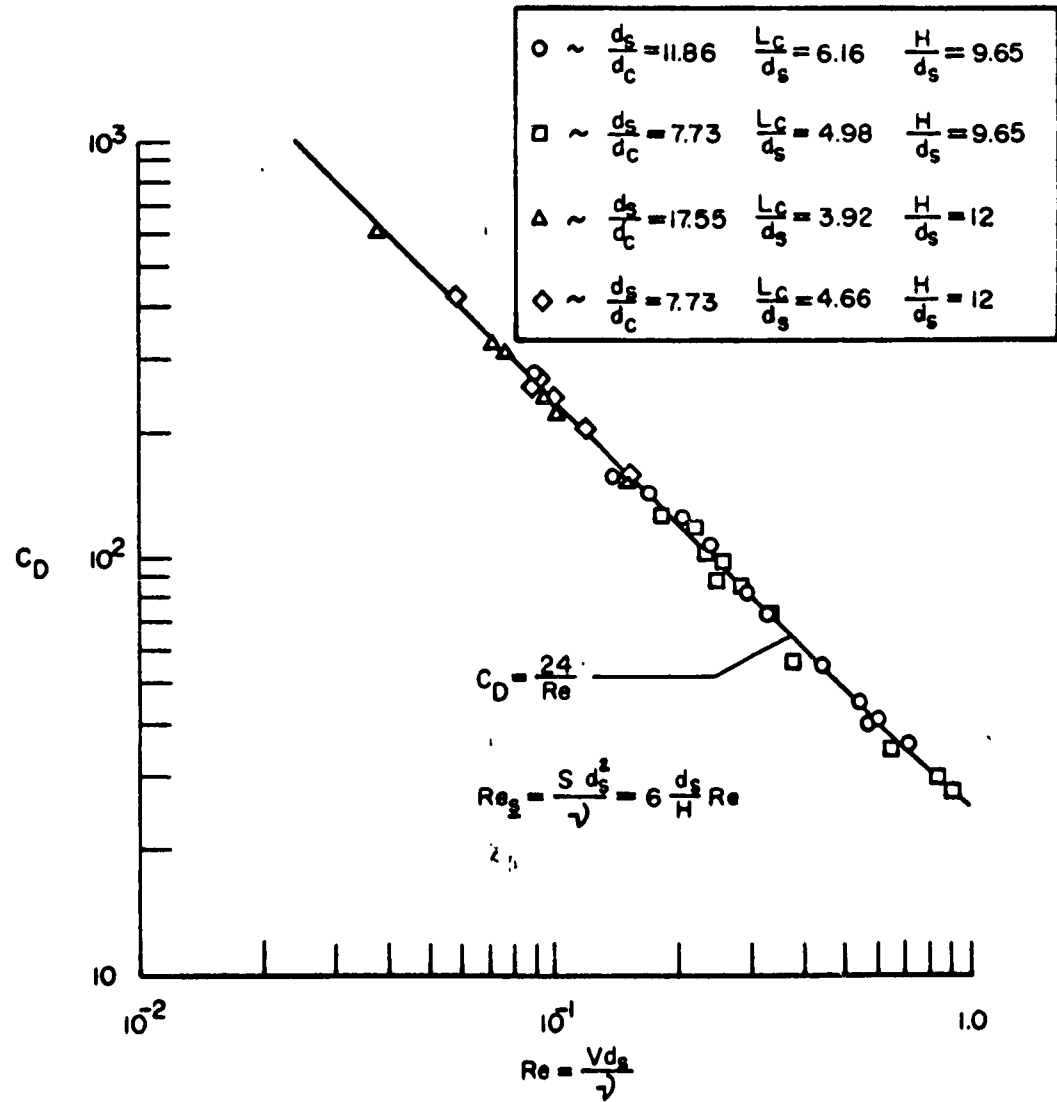


Fig. 33 - Drag of a Sphere in Shear Flow

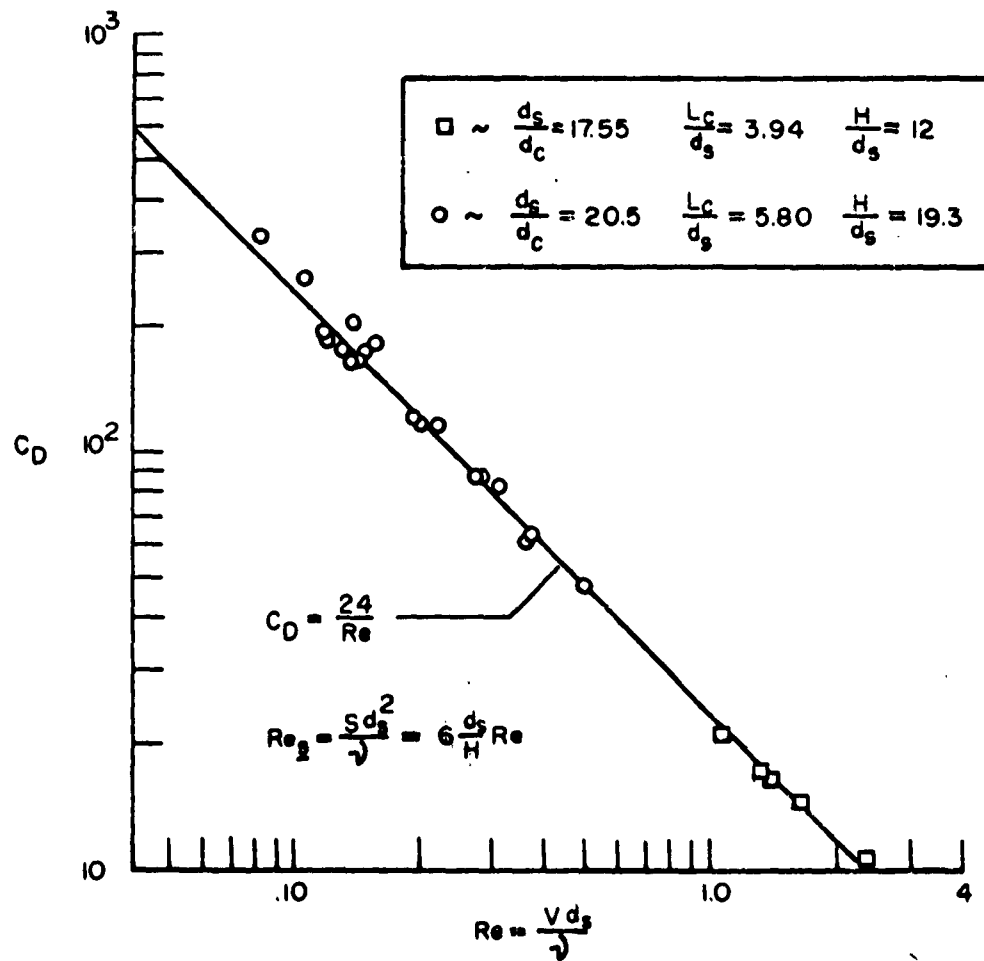


Fig. 34 - Drag of a Sphere in Shear Flow

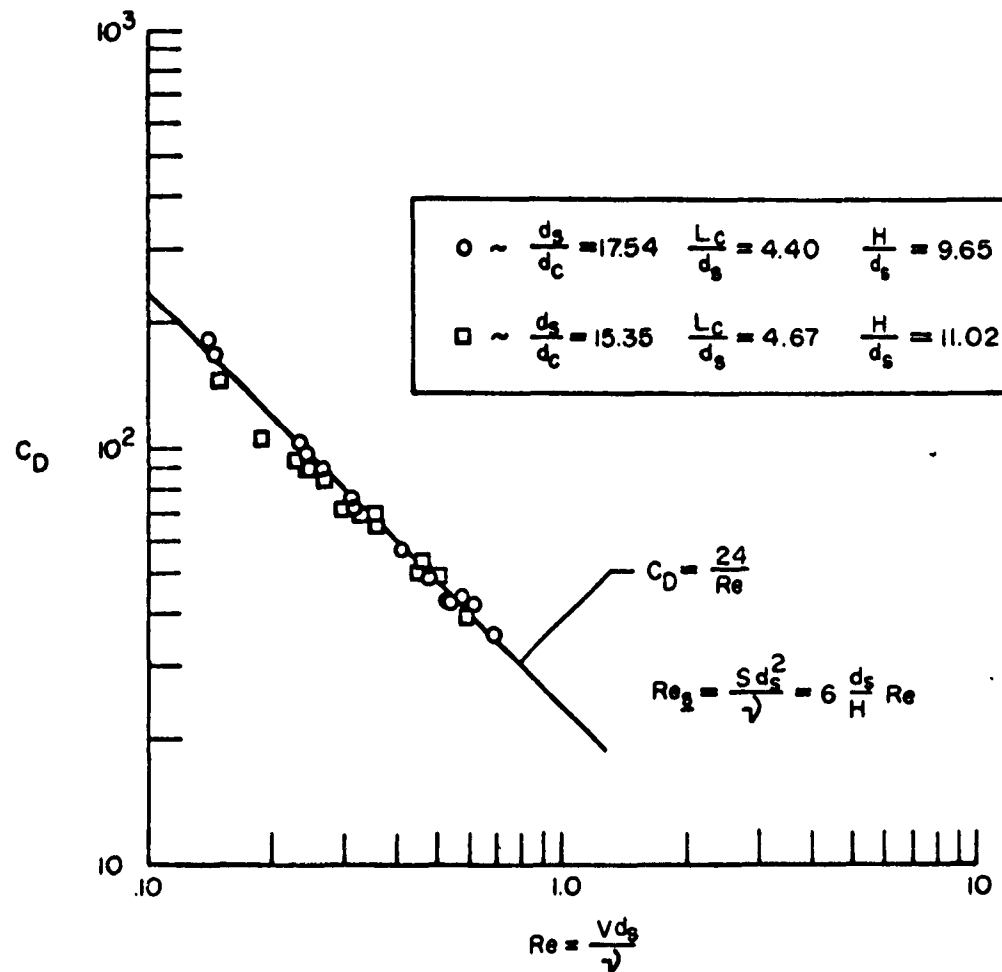


Fig. 35 - Drag of a Sphere in Shear Flow

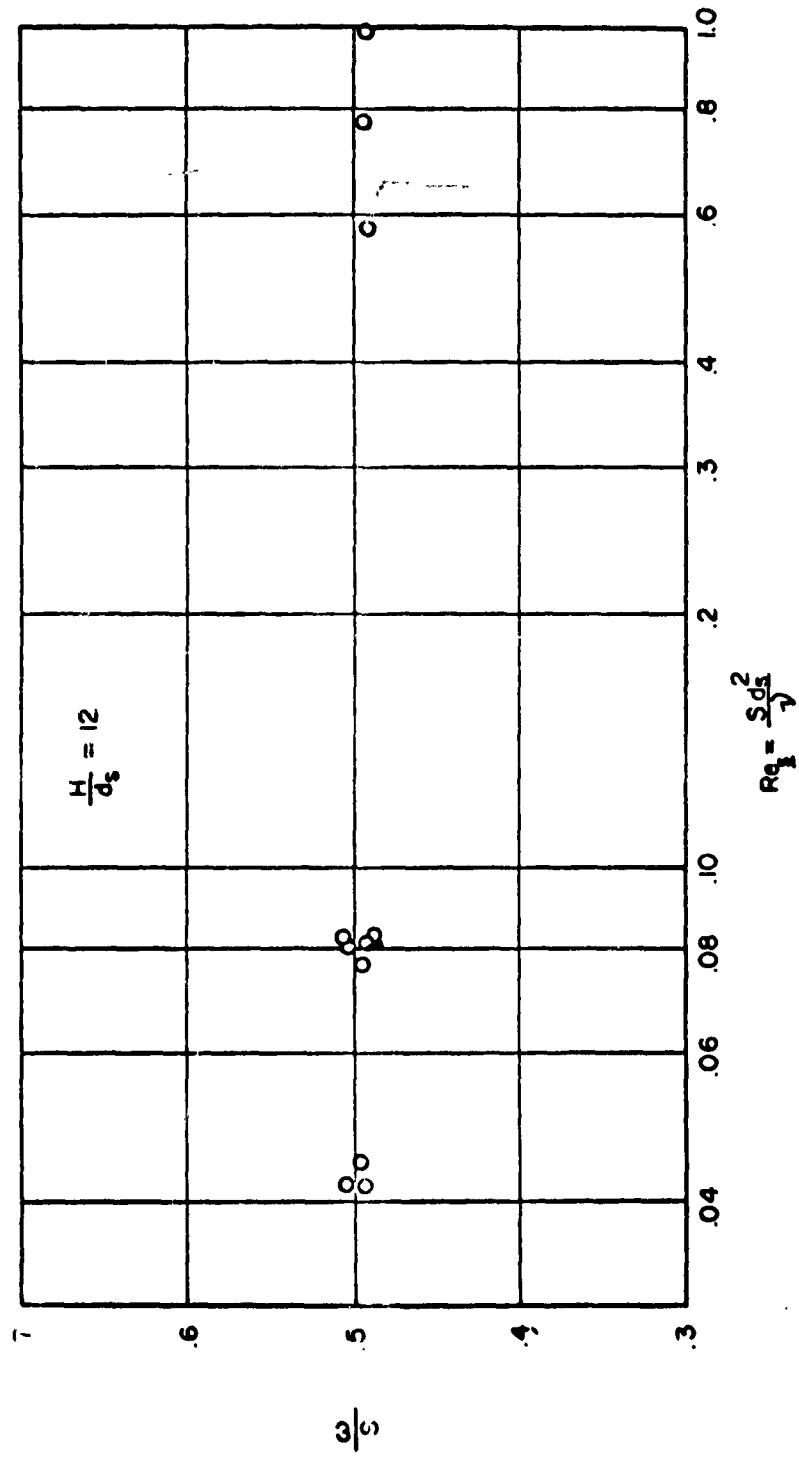
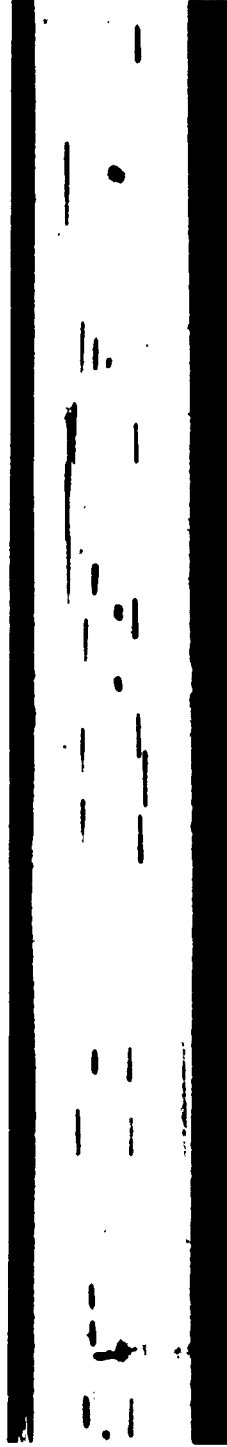


FIG. 36 - Rotation Rate of a Free Sphere in Uniform Shear Flow



$Re_B = 166$



$Re_B = 569$

Fig. 37 - Streak Photographs of Shear Flow, $\frac{\Delta}{H} = 13$

 $Re_s = 721$

Fig. 38 - Streak Photograph of Shear Flow, $\frac{A}{H} = 13$

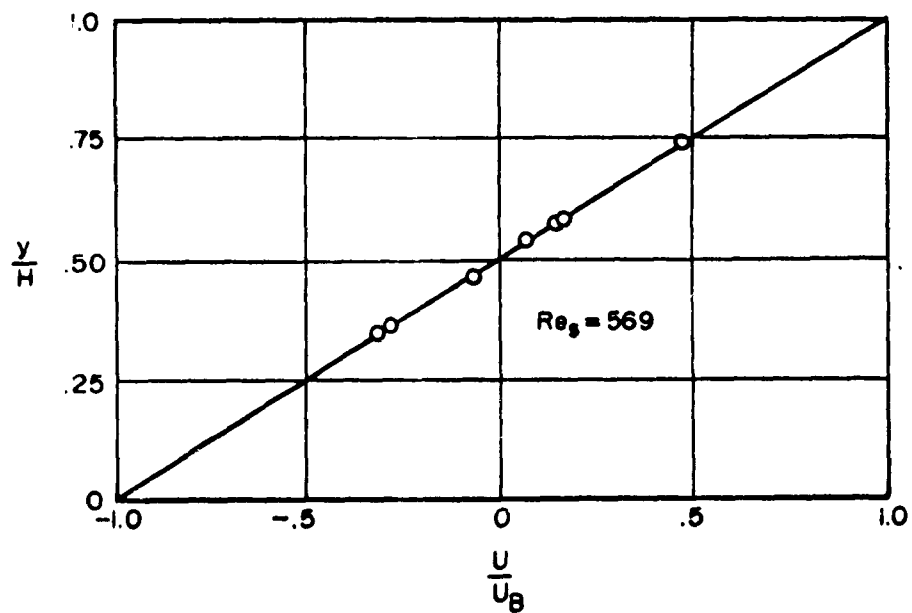
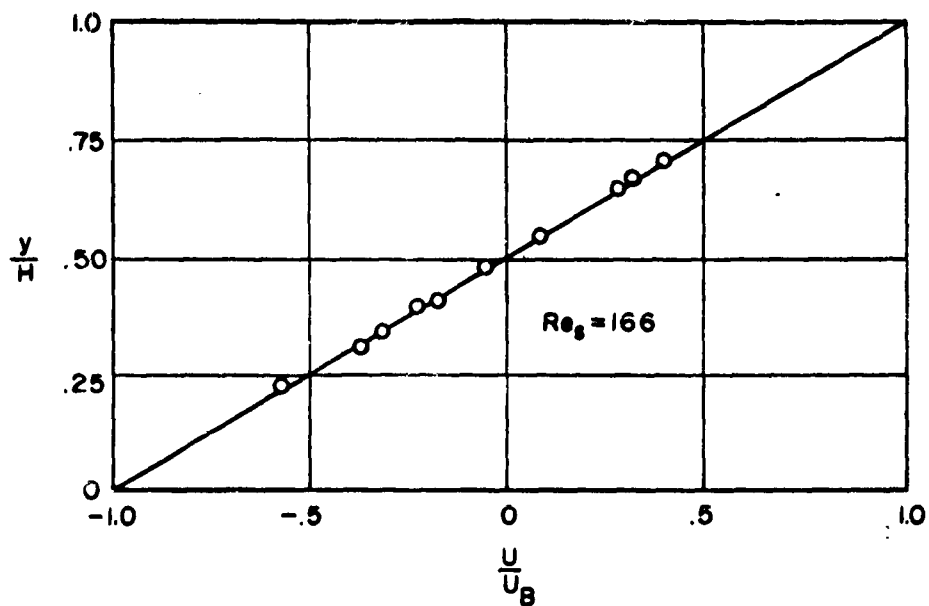


Fig. 39 - Velocity Profiles, $\frac{\lambda}{H} = 13$

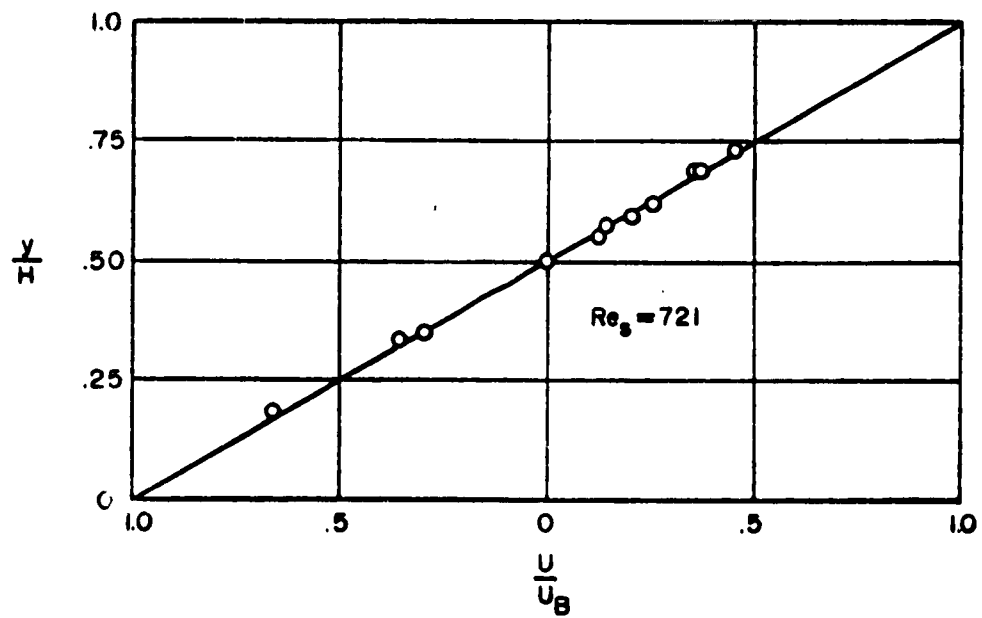


Fig. 40 - Velocity Profile, $\frac{\Delta}{H} = 13$



(a)

 $Re_s = 885$ 

(b)

 $Re_s = 1260$

Fig. 41 - Streak Photographs of Rectilinear Couette Flow



(a)

 $Re_s = 13,500$  $Re_s = 17,000$
(b)

Fig. 42 - Streak Photographs of Rectilinear Couette Flow



(a)

 $Re_g = 20,800$ 

(b)

 $Re_g = 32,000$

Fig. 43 - Streak Photographs of Rectilinear Couette Flow

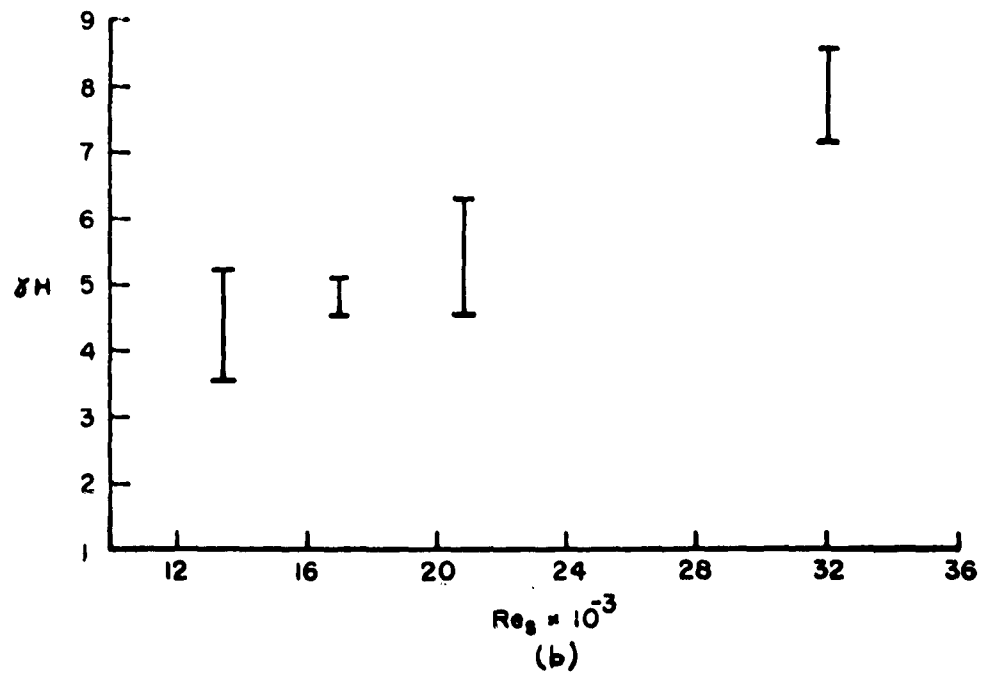
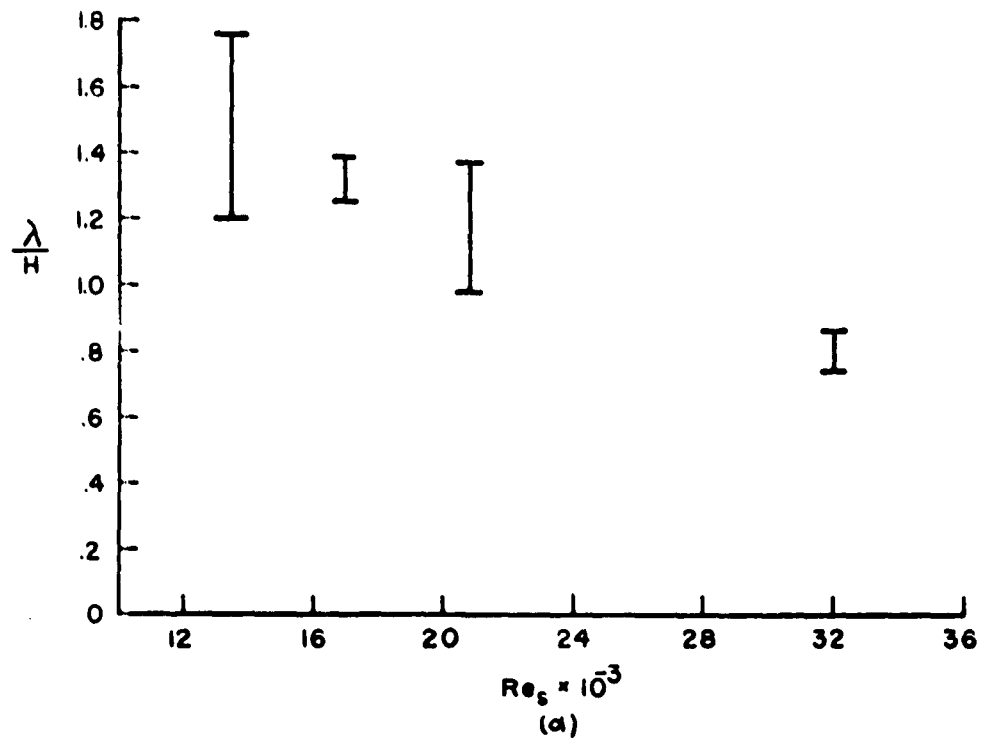


Fig. 44- Wavelength and Wave Number of Primary Instability in Couette Flow

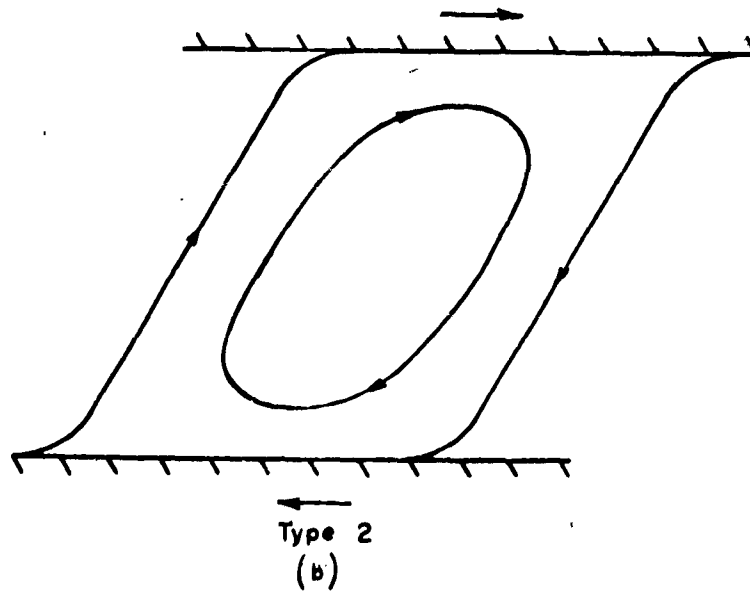
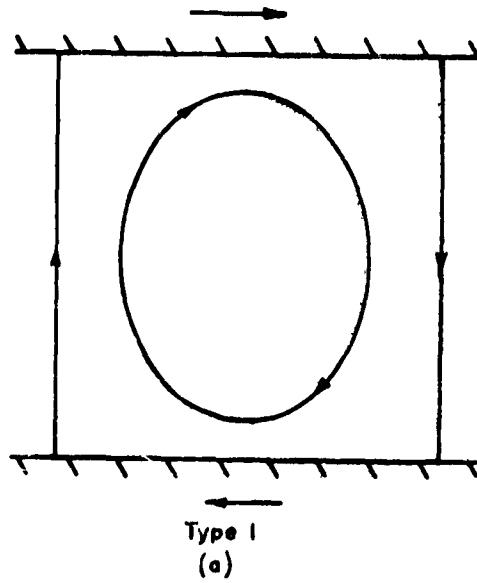


Fig. 45 - Modes of Oscillations in Plane Couette Flow (Hopf)

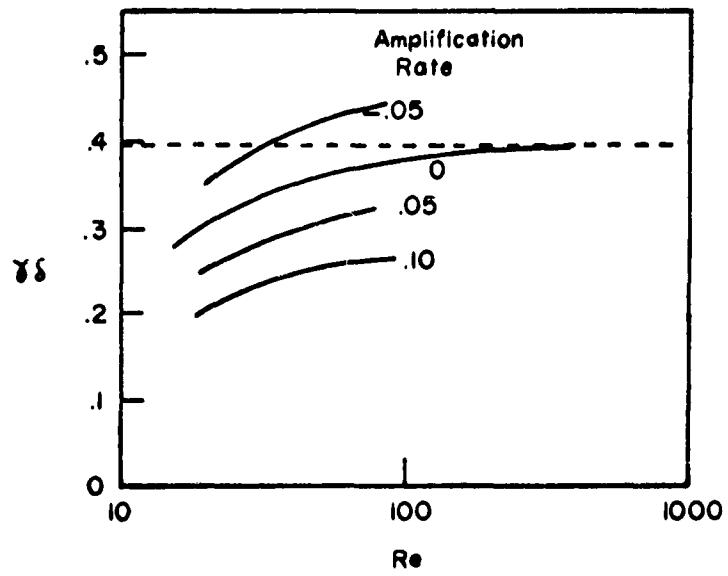


Fig. 46 - Stability Characteristics in Parallel Stream Mixing Region (Lessen)

BIOGRAPHICAL SKETCH

David L. Kohlman was born on October 13, 1937, in Houston, Texas. After graduation from Guelph Collegiate Institute, Guelph, Ontario, Canada, he attended Graceland College (Lamoni, Iowa) from which he received an Associate in Arts degree in 1957. The author then studied aeronautical engineering at the University of Kansas where he graduated "with highest distinction" in 1959 with a Bachelor of Science degree. Further study at the University of Kansas led to a masters' degree in aeronautical engineering in 1960. In the fall of 1960 he embarked on his doctoral program at M.I.T. For three years, beginning in 1959, the author was a Fellow of the National Science Foundation. His experience includes three summers with The Boeing Company, Wichita, Kansas, and one summer with the Sandia Corporation, Albuquerque, New Mexico. He is an associate member of the Institute of the Aerospace Sciences, and holds membership in Tau Beta Pi, Sigma Tau, and Sigma Gamma Tau, honorary engineering fraternities. The author is married and has one son.